The Thesis Committee for Miguel Cisneros
Certifies that this is the approved version of the following thesis:

An experimental calibration of chlorine isotope fractionation between amphibole and fluid at 700 °C and 0.2 GPa

APPROVED BY
SUPERVISING COMMITTEE:

Supervisor:

Jaime Barnes

James Gardner

William Carlson

An experimental calibration of chlorine isotope fractionation between amphibole and fluid at 700 °C and 0.2 GPa

by

Miguel Cisneros, B.S.

Thesis

Presented to the Faculty of the Graduate School of

The University of Texas at Austin

in Partial Fulfillment

of the Requirements

for the Degree of

Master of Science in Geological Sciences

The University of Texas at Austin

August 2013

Dedication

This thesis is dedicated to all the wonderful people I've had the privilege to come across in my life. To my parents, family, friends, and colleagues: this feat would have been impossible without your encouragement.

Acknowledgements

Words can't express my gratitude for the many positive individuals I've been privileged to have in my life. To my parents: this journey would have been impossible without your support. The numerous sacrifices you burdened upon yourself gave me the opportunity to succeed. Your resilience through hardships is most admirable and has been a source of motivation during many late nights in the laboratory. To my friends and family: you keep my life moving outside of the office/lab and always keep my feet grounded, thank you. Stable isotope group: thank you, for reminding me daily that science should be first and foremost, fun.

To my committee and scientific mentors: thank you for always guiding me through my scientific inquiries and difficulties. Jim Gardner provided invaluable support in the experimental lab. Bill Carlson greatly improved the tenor of this thesis; any remaining errors are trivial compared to those he repaired! Dave Jenkins was an instrumental part of this work, having provided me with the knowledge to confidently delve into the world of amphibole synthesis. Experimental work has truly been a humbling experience, and I applaud those individuals whom have made a career of it! Lastly, Jaime Barnes, my superb advisor, was persistent with her numerous revisions of this thesis, outstanding mentorship, and personal guidance. I'm glad, and lucky enough to be able to call Jaime a lifelong friend.

This work was supported by the National Science Foundation and a University of Texas at Austin Graduate School Fellowship. I also gratefully acknowledge the Jackson School of Geosciences for its unmatched financial support, and especially Philip Guerrero, for his helpful guidance with all important paperwork.

Abstract

An experimental calibration of chlorine isotope fractionation between amphibole and fluid at 700 °C and 0.2 GPa

Miguel Cisneros, M.S. Geo. Sci.

The University of Texas at Austin, 2013

Supervisor: Jaime Barnes

A Cl stable isotope fractionation factor between amphibole and fluid has been determined at 700 °C and 0.2 GPa. Rates of isotope exchange between pargasite and water at 600-800 °C were slow; therefore synthesis of amphibole in the presence of a fluid was necessary to facilitate the incorporation of Cl into amphibole. Hastingsite was synthesized from an oxide mixture and reacted with a NaCl-bearing supercritical fluid for periods of 3 to 14 days, approximately at the wüstite-magnetite buffer. Based on these synthesis-reaction experiments, the fractionation between hastingsite and a NaCl-bearing solution (~20000 ppm Cl) at 700 °C is $10^3 \ln\alpha_{amphibole\text{-}fluid} = 0.19‰ \pm 0.23‰$. These data display near zero fractionation at 700 °C, but suggest that amphibole is slightly enriched in ^{37}Cl relative to the fluid, in agreement with empirical and theoretical results.

Table of Contents

List of Tables ix

List of Figures x

Chapter 1: Introduction 1

Chapter 2: Background 5

2.1 Natural chlorine isotope variation 5

2.2 Methodology 5

2.3 Results of prior synthesis experiments 7

2.4 Choosing a starting composition 8

2.5 Driving forces of isotope exchange 10

Chapter 3: Methods 12

3.1 Synthesis experiments 12

3.1.1 Starting materials 12

3.1.2 Experimental techniques 14

3.2 Chlorine isotope analysis 17

3.2.1 Chlorine extraction 17

3.2.2 IRMS measurement 18

3.3 X-ray diffraction 18

3.4 Electron microprobe 19

Chapter 4: Results 21

4.1 Synthesis products 21

4.1.1 XRD and EPMA results 21

4.1.2 SEM imaging of synthesis products 22

4.2 Fractionation experiments 28

Chapter 5: Discussion 33

5.1 Recommended fractionation factor 33

5.2 Comparison to theoretical results 37

5.3 Comparison to empirical results 37

Chapter 6: Conclusions 39

Appendix A Figures 40

Appendix B Tables 46

References 50

List of Tables

Table 1: Bulk compositions of staring mixtures 13

Table 2: Synthesis conditions and experimental products 24

Table 3: Average compositons of synthetic amphiboles.....27

Table 4: Cl isotope data for amphibole-water fractionation experiments.....30

Table B1: Electron-probe microanalysis (wt%) of standards 46

Table B2: Electron-probe microanalysis (wt%) of standards 47

Table B3: Cl isotope data for pargasite-water fractionation experiments 48

Table B4: Fractionation-factor best-fit equations.....49

List of Figures

Figure 1: Experimental set-up for synthesis-reaction experiments 16

Figure 2: SEM images of synthesis products 25

Figure 3: Classification scheme for calcic amphiboles 26

Figure 4: $\delta^{37}Cl$ values of hastingsite vs. time 31

Figure 5: $10^3 ln\alpha_{amphibole\text{-}fluid}$ values of amphibole-fluid pairs vs. time 32

Figure 6: $10^3 ln\alpha_{amphibole\text{-}fluid}$ values of amphibole-fluid pairs vs. time 36

Figure A1: Cl isotope variation of terrestrial samples 40

Figure A2: $10^3 ln\alpha_{mineral\text{-}water}$ values vs. time for synthesis-reaction experiments 41

Figure A3: $10^3 ln\alpha_{pargasite\text{-}fluid}$ values of pargasite-fluid pairs vs. time 42

Figure A4: $10^3 ln\alpha_{zoisite\text{-}water}$ vs. temperature 43

Figure A5: X-ray diffraction pattern of hastingsite.....44

Figure A6: Reduced partition function ratios for alkali-chloride salts.....45

Chapter 1: Introduction

Secondary silicate minerals (e.g., amphibole, chlorite, serpentine) found within oceanic crust and lithospheric mantle are enriched in chlorine (up to 4 wt% Cl) during hydrothermal alteration (e.g., Ito et al., 1983; Vanko, 1986; Philippot et al., 1998). In addition, the Cl isotope ratios ($^{37}Cl/^{35}Cl$) of altered oceanic crust and lithospheric mantle differ from the isotopic signatures of major chlorine reservoirs (e.g., Magenheim et al., 1995; Barnes et al., 2006; Bonifacie et al., 2008a; Selverstone and Sharp, 2011; Barnes and Cisneros, 2012). Theoretical calculations have estimated minimal fractionation between amphibole and fluid at temperatures pertinent to hydrothermal alteration (Schauble et al., 2003); however, supplementary experimental studies of Cl isotope fractionation between any silicate mineral and fluid do not exist. In order to understand processes responsible for isotopic fractionation between chlorine reservoirs and the host rock of interest, and to resolve the origin of fluids responsible for alteration, an experimental calibration of chlorine isotope fractionation during fluid-rock interaction is necessary. Determining Cl isotope partitioning among silicates and fluid will also elucidate temperatures of equilibration during hydrothermal alteration.

The processes that control Cl isotope partitioning during hydrothermal alteration have been difficult to constrain, due to our limited understanding of Cl isotope fractionation throughout the isotopic evolution of the interacting fluid and during fluid-rock interaction. Experimental work is restricted to determining Cl isotope fractionation during evaporation and distillation (Sharp et al., 2010a), evaporite precipitation (Eggenkamp et al., 1995; Liebscher et al., 2006), diffusion in water (Richter et al., 2006), and ion filtration (Campbell, 1985). Chlorine isotope partitioning between phases during

processes such as sub- or super-critical two-phase fluid separation, adsorption, and fluid-silicate rock interaction has not been calibrated experimentally. Theoretical studies providing estimates of Cl isotope fractionation between phases have predated experimental work. Seminal studies focused on determining Cl isotope partitioning among gaseous substances (Urey, 1947; Richet et al., 1977). More recent work has focused on determining reduced partition function ratios for isotope exchange of alkali-chloride salts, such as $FeCl_2$ and $MnCl_2$ (analogs for silicates) and NaCl (Schauble et al., 2003). Amphiboles and micas are proposed to be best represented by $FeCl_2$, due to the similarity in coordination environments between Cl^- in $FeCl_2$ (Cl bonded to three Fe^{2+} ions, ~2.50 Å distance) and Cl^- in amphiboles/micas (Cl bonded to three M sites, ~2.46 Å distance). Results suggest that ^{37}Cl preferentially partitions into amphibole relative to coexisting fluid; however, minimal fractionation occurs at high temperatures. These calculations provide the best currently available estimate of fractionation between amphibole and solutions with Cl^- solvated by H_2O molecules.

Due to the high volatility, hydrophilic nature, and incompatible behavior of chlorine during silicate melting, chlorine is concentrated in the crust and as a result is the most abundant anion in the Earth's exosphere, that is, its crust, ocean, and atmosphere (Turekian and Wedepohl, 1961). The high solubility of chlorine in water makes it a valuable element for understanding fluid-mediated processes (Wiberg, 2001); therefore, much focus has been directed towards implementing chlorine isotopes as fluid tracers (e.g., Barnes et al., 2006a; Barnes and Sharp, 2006; Barnes et al., 2009a; Selverstone and Sharp, 2011). Several studies have based important conclusions on the assumption that minimal fractionation exists between silicates and NaCl-dominated brines at elevated temperatures (e.g., Barnes et al., 2006a; Barnes et al., 2008; Barnes et al., 2009a; Barnes

and Straub, 2010; Selverstone and Sharp, 2011). Mid-Atlantic Ridge and East Pacific Rise ridge-axis high-temperature hydrothermal fluids have shown near constant Cl isotope ratios (similar to seawater) yet varying Cl concentrations, implying minimal Cl isotope fractionation during fluid phase separation (Bonifacie et al., 2005). Recent studies have therefore assumed that oceanic crust interacts with fluids containing isotopic values similar to that of seawater. Amphibole-rich altered oceanic crust (AOC) basalts (hole 504B) on average yield positive Cl isotope values that are in general agreement with theoretically determined equilibrium fractionation between a silicate (amphibole) and a fluid (seawater) (Barnes and Cisneros, 2012). However, others have recorded AOC basalt (hole 504B) with negative Cl isotope values (Bonifacie et al., 2007a), wherein the solid becomes depleted in ^{37}Cl relative to the fluid, in discrepancy with general rules of mass-dependent fractionation. The two studies show conflicting results that have been difficult to resolve. Due to limited experimental calibrations, natural processes that operated in fractionating Cl stable isotopes have been difficult to quantify.

The purpose of this study is to provide experimental constraints on the magnitude of chlorine isotope fractionation between a calcic amphibole and fluid. Amphibole was chosen as the mineral of interest because it is one of the most abundant silicate hosts of chlorine in crustal environments (e.g., Ito et al., 1983; Straub and Layne, 2003). Often, isotopic exchange between a hydrous silicate mineral and fluid is slow, even at temperatures $\geq$ 500 °C (e.g., O'Neil and Taylor, 1969; Matthews et al., 1983b). To overcome slow kinetic rates of exchange reactions, synthesis experiments are implemented as a substitute for isotope exchange experiments. Synthesis reaction experiments between a mineral and fluid, involve the solid incorporating an isotopic composition similar to that of the fluid during initial growth. After mineral precipitation,

synthesis experiments typically involve a short duration of isotope exchange, after which a fractionation factor can be determined (Clayton et al., 1972; Matthews et al., 1983b; O'Neil, 1986). An experimental study of equilibrium Cl isotope fractionation between an amphibole and fluid is necessary to supplement theoretical calculations, as $FeCl_2$ and NaCl do not fully represent the crystallography of amphiboles and Cl^- solvated by H_2O. Determination of equilibrium fractionation factors between hydrous minerals and co-existing fluid will help decipher temperatures of equilibration, origin of hydrothermal fluids, and ultimately aid in the understanding of processes controlling Cl isotopes during hydrothermal alteration.

Chapter 2: Background

2.1 NATURAL CHLORINE ISOTOPE VARIATION

Chlorine has two stable isotopes, ^{35}Cl and ^{37}Cl, with relative abundances of 75.77% and 24.23%, respectively (Parrington et al., 1966). Cl isotope variations are reported as $\delta^{37}Cl_{sam} = (R_{sam}/R_{std} - 1)*10^3$, where R_{sam} and R_{std} are the $^{37}Cl/^{35}Cl$ ratios of the sample and seawater standard, respectively. The range of Cl isotope values in natural whole rock, fluid, and gas samples is shown in Fig. A1. $\delta^{37}Cl$ variation among terrestrial samples ranges from approximately -8‰ to +20‰ (Ransom et al., 1995; Rizzo et al., 2013). Values of -8‰ are restricted to sedimentary pore fluids (Ransom et al., 1995; Spivack et al., 2002; Godon et al., 2004). Values as high as +20‰ are restricted to fumarole gases with Cl isotope values that result from kinetic fractionation between vapor-liquid phases at temperatures > 100 °C, following condensation on cooler fumarole walls (Barnes et al., 2009b; Sharp et al., 2010a; Rizzo et al., 2013).

2.2 METHODOLOGY

Isotopic differences between two species can be expressed by a fractionation factor ($\alpha_{mineral\text{-}fluid}$):

$$\alpha_{mineral\text{-}fluid} = \left(\frac{1000 + \delta_{mineral}}{1000 + \delta_{fluid}} \right) \quad (1)$$

or

$$10^3 \ln\alpha_{mineral\text{-}fluid} \approx \Delta_{mineral\text{-}fluid} \quad (2)$$

where $\delta_{mineral}$ and δ_{fluid} denote the isotopic composition of the mineral and fluid phases in standard δ notation, respectively, and $\Delta_{mineral\text{-}fluid} = \delta_{mineral} - \delta_{fluid}$. Equation 2 is a good approximation only when $\Delta_{mineral\text{-}fluid} < 10‰$ (Sharp, 2007); consequently all final fractionation factors are reported here as $10^3 \ln\alpha_{mineral\text{-}fluid}$.

The approach in this study is synthesis of an amphibole in the presence of a Cl-bearing solution, measuring isotopic fractionation in multiple experiments with increasing durations. The method differs from "true isotope-exchange" experiments (Clayton et al., 1972; O'Neil, 1986). Isotope-exchange experiments consist of reacting a mineral powder with a solution at a fixed pressure and temperature, in an attempt to produce transfers of isotopes between the two phases until equilibrium partitioning is achieved. These types of experiments have been the most common way of determining fractionation factors between mineral-water pairs. Northrop and Clayton (1966) successfully completed isotope-exchange experiments by employing a "two-directional approach" to achieve equilibrium. The two-directional approach consists of equilibrating a mineral (e.g., quartz with an initial $\delta^{18}O$ value of +2‰) with two solutions having δ values greater and less than that of the mineral (e.g. initial $\delta^{18}O_{fluid}$ = +10‰ and -5‰). The system approaches equilibrium with increasing time, and when $\Delta_{qtz\text{-}water}$ ($\delta^{18}O_{qtz} - \delta^{18}O_{water}$) values are equal for both quartz-water systems, equilibrium has been reached. True isotope-exchange experiments are predominantly driven by free-energy differences related to isotope substitution, making this form of experiment the most reliable for determining fractionation factors (O'Neil, 1986). However, other experimental techniques are needed when kinetic rates are slow (e.g., low temperatures, slow volume-diffusion rates). These techniques include: (a) crystallization of a metastable phase (e.g., SiO_2 gel or glass) (O'Neil and Taylor, 1969; Clayton et al., 1972; Matthews et al., 1983b); (b) crystallization of new phase during a polymorphic transition (Clayton et al., 1975); or (c) crystallization of a new phase from an oxide mixture ("synthesis-reaction" experiments) (O'Neil, 1986). Experiments employing these techniques have been carried out with reasonable success, as explained in the following summary of prior results

(Clayton et al., 1972; O'Neil, 1986; Carothers et al., 1988; Yapp, 1990; Skulan et al., 2002).

2.3 RESULTS OF PRIOR SYNTHESIS EXPERIMENTS

Clayton et al. (1972) reacted metastable silica gel at low temperatures (≤ 500 °C) to determine oxygen isotope fractionation factors between quartz and water. The underlying problem with early synthesis experiments (i.e., Clayton et al., 1972) is that fractionation between synthesized quartz and water resulted in a fractionation factor that differs from that of direct isotope-exchange experiments. Several studies (e.g., Clayton et al., 1972; Saccocia et al., 2009) were also able to approach $\Delta_{\text{mineral-fluid}}$ equilibrium values from only one direction. $\Delta_{\text{mineral-fluid}}$ would have the same value after the first measurement (first measurement after time = 0), independent of the starting $\delta^{18}O$ value of the solution (Fig. A2). Authors have argued that a one-directional approach to constant $\Delta_{\text{mineral-fluid}}$ values is not indicative of isotopic equilibrium (O'Neil, 1986). Additionally, when completing high-temperature cold-seal-pressure-vessel synthesis experiments it is difficult to disprove isotopic heterogeneity (unless in situ techniques are available) and the possibility of kinetic fractionation overprinting equilibrium fractionation.

Studies following that of Clayton et al. (1972) achieved greater success with synthesis experiments. Carothers et al. (1988) was the first to successfully determine oxygen isotope fractionation between siderite ($FeCO_3$) and water using a synthesis-reaction experiment from 33° to 197 °C. The authors were able to demonstrate that their synthesis experiments did not undergo kinetic isotope fractionation due to differing diffusion rates of oxygen isotopes or during crystallization, and furthermore did not create isotopic heterogeneity in the siderite. Further work (e.g., Yapp, 1990; Skulan et al., 2002; Pearce et al., 2012) has successfully completed synthesis isotope fractionation

experiments with other elements, such as Fe and Mg. Importantly, Mg isotope fractionation experiments have clearly demonstrated that equilibrium fractionation can overprint kinetic isotope fractionation that occurs during dissolution and crystallization (assuming isotopic equilibrium is reached), especially at high temperatures (Pearce et al., 2012; Macris et al., 2013); however, further conclusive evidence showing that equilibrium fractionation is always the dominant form of isotope partitioning does not exist.

2.4 CHOOSING A STARTING COMPOSITION

Preliminary isotope-exchange experiments in this study between a Cl-bearing solution and a natural pargasite from the Finero Complex, Western Alps, Italy [$(Na_{0.4}K_{0.1})(Ca_{1.8}Na_{0.2})(Mg_{3.5}Fe^{3+}_{0.8}Al_{0.6})(Al_{1.9}Si_{6.1})O_{22}(OH,Cl)_2$] revealed that Cl isotope exchange rates at 600 °C and 50 MPa are sluggish: even after ~ 1 month, isotopic compositions did not converge to consistent values (Fig. A3). High Mg concentrations in the pargasite likely also contributed to slow volume-diffusion rates, due to the well-known Mg-Cl avoidance principle (see below). To increase kinetic rates and to facilitate the incorporation of Cl into amphibole, an "ideal" amphibole composition was synthesized. The "ideal" composition is enriched in Fe^{2+}, K, Na and Al for reasons addressed below and is a composition representative of AOC amphiboles. This composition allows for faster equilibration times, increased Cl concentrations in amphibole, and the ability to vary amphibole composition to investigate compositional effects on Cl isotope partitioning. Higher Cl concentrations in amphiboles allow for more precise EPMA and IRMS measurements. In order to decrease the time necessary to reach equilibrium and to be able to synthesize amphibole, I carried out experiments at higher temperatures than those normally prevailing during hydrothermal alteration of oceanic

crust (~30-500 °C) (Staudigel, 2003). Chlorine isotope fractionation extrapolations to lower temperatures could then be achieved based on an empirical equation determined at higher temperatures; however, extrapolation of high-temperature experiments to estimate fractionation factors at low temperatures should be approached with caution. Experimental and theoretical studies have shown conflicting behavior between mineral-fluid fractionation at high and low temperatures (Fig. A4).

The amphibole compositions of interest for synthesis varied from ferro-pargasite to hastingsite (e.g., $NaCa_2Fe_4^{2+}Fe^{3+}Si_6Al_2O_{22}(OH)_2$). Considerable debate about the method of Cl^- incorporation in amphiboles is present in the literature (Munoz and Swenson, 1981; Volfinger et al., 1985; Morrison, 1991; Oberti et al., 1993; Zhu et al., 1994; Mazdab, 2003). Chloride anions reside in the amphibole O3 site by replacement of OH^- molecules. Calcic amphiboles that contain up to 7.24 wt% Cl are known to exist in nature (Krutov, 1936). The reason for chlorine variation in amphiboles is more enigmatic. The large difference in ionic radii between Cl^- and OH^- (1.81 Å and 1.35 Å, respectively), has been a fundamental problem with direct substitution between anion pairs and was first addressed in micas (Munoz, 1984). Several characteristics about amphiboles with high Cl concentrations are observed nearly universally. Cl concentration increases proportionately with increasing Fe^{2+}, K, Na and Al contents and is inversely proportional to Mg apfu (atoms per formula unit), the latter having been termed the Mg-Cl avoidance rule. Volfinger et al. (1985) argue that Fe^{2+} enlarges the octahedral sheet and eases the introduction of Cl into the O3 site. Munoz (1984) suggests that the greater strength of Fe-Cl in comparison to Mg-Cl bonds leads to preferential incorporation of Cl. Aside from structural controls, some suggest that elevated Cl concentrations in hydrous silicates are likewise a function of fluid chlorinity, pH, and temperature (e.g. Vanko,

1986; Liu et al., 2009). To conform with empirical observations, the "ideal" amphibole composition required high Fe^{2+}, Al, Na, and K concentrations and negligible Mg to incorporate the maximum amount of Cl.

2.5 DRIVING FORCES OF ISOTOPE EXCHANGE

Stable isotope fractionation is mainly driven by zero-point energy differences of isotopically substituted molecules (Urey, 1947; Richet et al., 1977; Clayton, 1981; Chacko et al., 2001; Schauble, 2004). Classical thermodynamics provides a way to explore the difference in free energies between molecules of differing isotopic species. For any chosen isotopic exchange reaction, the relationship

$$-RT\ln K = \Delta G_{rxn}^{T,P} = \Delta H_{rxn}^{0} - T\Delta S_{rxn}^{0} + P\Delta V_{rxn}^{0} \quad (3)$$

in which R is the gas constant, K is the equilibrium constant, G is Gibbs free energy, ΔH_{rxn}^{0} is the enthalpy of formation (where the superscript ° denotes that the value is for standard-state pressure and temperature, T = 298.15 K and P = 1 bar), T is temperature, ΔS_{rxn}^{0} is the change in entropy of the reaction, P is pressure, and ΔV_{rxn}^{0} is the volume change of the reaction, can be used to identify the energetically favorable molecule, the one that produces a state with the lowest Gibbs free energy. ΔH_{rxn}^{0} measures the heat of formation given off when an isotope substitution occurs, therefore systems favor isotopologues with the lowest ΔH_{rxn}^{0} (i.e., strongest bonds). Statistical-mechanics calculations have demonstrated that isotope fractionation is strongly temperature dependent (i.e., Urey, 1947; Bigeleisen and Mayer, 1947). Rearrangement of equation 3 illustrates that at infinite temperature, equal distribution of isotopes amongst species is favored (fractionation is 0).

$$-\frac{\Delta G_{rxn}^{P,T}}{RT} = \ln K \quad (4)$$

The last term in equation 3 shows that isotopes with the smallest molar volumes are favored at high pressures (molar volume increases with mean bond length). However, the difference between molar volumes of isotopically substituted molecules is minimal, and this term is non-important except in the case of hydrogen isotopes (Polyakov and Kharlashina, 1994; Horita et al., 1996; Horita et al., 1999). For this reason, the present experiments have been carried out at constant pressure because pressure-dependent isotope fractionation should be negligible with Cl isotopes.

Chapter 3: Methods

3.1 SYNTHESIS EXPERIMENTS

3.1.1 STARTING MATERIALS

Starting mixtures were prepared from reagent-grade SiO_2, Na_2CO_3, $CaCO_3$, Al_2O_3, Fe_2O_3 and metallic Fe (Fe°). Oxides used for synthesis of amphibole were prepared following the procedures of Jenkins and Bozhilov (2003). SiO_2 was prepared by desiccation of silicic acid ($SiO_2 \cdot nH_2O$) in a furnace at atmospheric pressure. Dehydration was carried out in steps at 400 $^{\circ}$C, 600 $^{\circ}$C, and 800 $^{\circ}$C, for 1 hour at each temperature, and lastly at 1100 $^{\circ}$C for ~24 hours. The final product is partially crystallized cristobalite as confirmed by X-ray diffraction (XRD). Appropriate oxides for the amphibole of interest were mixed in correct stoichiometric proportions and ground in acetone until fine and well mixed. Non-iron bearing reagents (SiO_2, Na_2CO_3, $CaCO_3$, and Al_2O_3) were mixed first and heated to 900 °C in a furnace for ~30 min to produce decarbonation of Na_2CO_3 and $CaCO_3$. The carbonate-free oxide mixture was weighed, and Fe_2O_3 and Fe° were then added in appropriate stoichiometric proportions, depending on the Fe^{2+}/Fe^{3+} ratio desired. Fe° is used to maximize the amount of ferrous iron produced in the amphibole. Fe is oxidized when reacted with H_2O sealed in the capsule; therefore, introducing an environment that is initially more reduced increases the probability of producing ferrous iron. Starting bulk compositions used are given in Table 1. Cl-bearing solutions consisted of seawater containing a $\delta^{37}Cl$ value of 0‰ (by definition) and a ^{37}Cl-enriched NaCl-bearing solution with a $\delta^{37}Cl$ value of +10.36‰. The seawater and high $\delta^{37}Cl$ solutions contain dissolved Cl^- concentrations of ~21000 ppm and 19000 ppm, respectively (measured by ion chromatography).

Table 1. Bulk compositions of starting mixtures

Sample Code	Bulk Composition	Reagents
HAST 1	$Na(Ca)_2(Fe_3^{2+},Fe^{3+},Al)(Al_2Si_6)O_{22}(OH,Cl)_2$	NaCl, $Ca(OH)_2$, Fe_2O_3, Fe°, Al_2O3, SiO_2
HAST 2	$Na_{0.5}K_{0.5}(Ca)_2(Fe_3^{2+},Fe^{3+},Al)(Al_2Si_6)O_{22}(OH)_2$	Na_2CO_3, K_2O, $Ca(OH)_2$, Fe_2O_3, Fe°, Al_2O3, SiO_2
HAST 3	$Na(Ca)_2(Fe_4^{2+},Fe^{3+})(Al_2Si_6)O_{22}(OH)_2$	Na_2CO_3, $CaCO_3$, Fe_2O_3, Fe°, Al_2O_3, SiO_2

3.1.2 EXPERIMENTAL TECHNIQUE

Experiments were carried out in cold-seal pressure vessels at 0.2 GPa and 700 °C, using water as a pressure medium. Temperature in the vessel was gauged using an external thermocouple. Approximately 150 mg of powder and ~30-150 mg of solution, depending on the fluid/rock ratio of interest (0.2 – 1.0, by mass), were loaded into $Ag_{70}Pd_{30}$ tubing. A fluid-to-rock (F/R) ratio between 0.2 to 1.0 was chosen for two reasons: (1) to provide enough water for complete conversion of the charge into amphibole, but to minimize the effects on incongruent dissolution of solids in the fluid phase [a F/R ratio of < 0.1 provides sufficient water to completely convert a charge to amphibole (Thomas, 1982)]; and (2) to provide sufficient Cl so that the mineral is isotopically homogenous. Ends of the capsules were welded shut by spot welding. Placing a wet Kimwipe across the metal joints helped to produce a porous-free weld. Water vapor produced during arc contact with metal displaces air and does not allow O_2 to dissolve into AgPd melt (Weidner, 1989). Capsules were placed in an oven at 110 °C for ~30 min to check for leaks. If mass loss occurred, the capsule was discarded. The AgPd capsule was placed in a Waspaloy vessel adjacent to a ~20 cm steel rod, and the remaining space was occupied by a Ni rod. An example of the experimental set-up is shown in Fig. 1. No buffer was employed to directly control f_{O_2}. The steel rod was used to reduce the f_{O_2} of the experiment to approximately the wüstite-magnetite buffer, as confirmed by an XRD scan of post-experiment steel rod coating. Experiments were quenched by removing the vessel from the furnace and cooling it with compressed air for ~3 min. The vessel was subsequently placed in a bucket with water. Samples were weighed after experiments to check for mass loss or gain. Capsules that had considerable gain in mass (> 1.0 mg) after a run were discarded. Many capsules lost mass during a run

(1 - 6 mg) but did not lose mass when placed in an oven after the run; therefore these experiments were still used to determine equilibrium Cl isotope fractionation. The reason for this mass loss during the experiment is unclear.

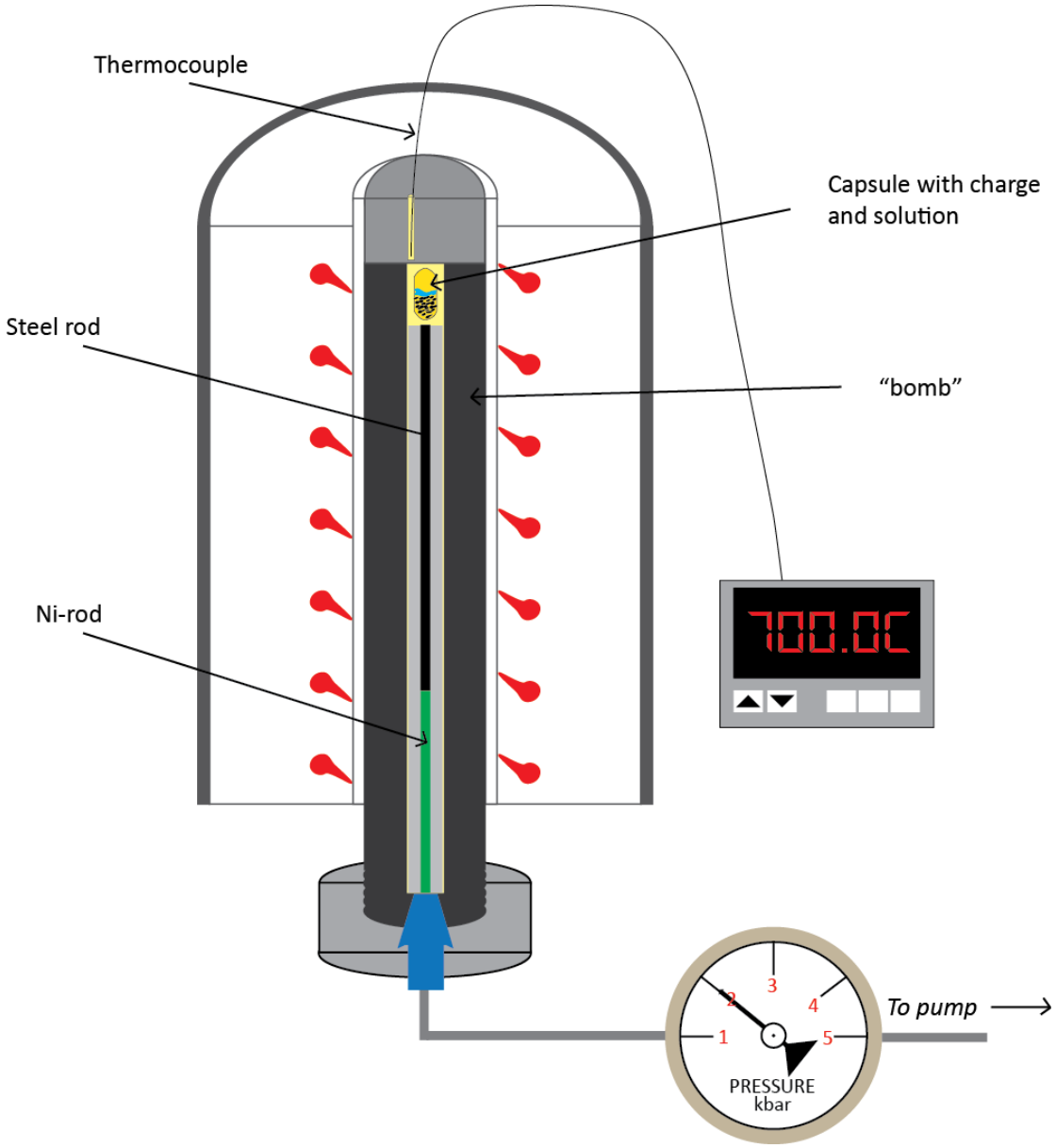

Figure 1. Experiment set-up for synthesis-reaction experiments. Experiments were carried out in cold-seal pressure vessels. A steel rod is placed adjacent to the AgPd capsule to reduce the f_{O_2} of the experiment. A Ni-rod is used as filler rod for the remaining volume of the vessel. Experiment conditions were 700 °C and 0.2 GPa.

3.2 CHLORINE ISOTOPE ANALYSIS

3.2.1 CHLORINE EXTRACTION

Experimental capsules were rinsed five times with 18 MΩ deionized (DI) water to remove surficial chloride. Clean capsules were subsequently submerged in a beaker filled with 18 MΩ DI H_2O and opened under water. The capsule was removed from and rinsed back into the beaker to collect any remaining synthesis product or Cl adsorbed to the capsule. The contents of the beaker were filtered through a 0.4 μm pore size filter allowing for collection of the synthesis products and the diluted experimental solution. The synthetic products were crushed into a fine powder with a mortar and pestle in an acetone solvent. After crushing, samples were washed and rinsed 3 times with ~ 30 mL of 18 MΩ deionized water to remove any possible surficial chlorine and allowed to dry in an oven at 60 °C overnight.

Chlorine was extracted from experimental amphibole products by pyrohydrolysis, following methods similar to Magenheim et al. (1995). Approximately 100 mg of powdered sample was loaded into quartz tubing, capped with quartz wool, and melted with an oxygen-gas flame torch. Chlorine is volatilized, transported in H_2O steam, and condensed in a cooling coil. H_2O with Cl^- solute is collected in a beaker and reacted with $AgNO_3$ for ~24 hours to produce AgCl. The remaining suspension is filtered, the beaker is rinsed with dilute HNO_3 (H_2O creates a colloidal substance with AgCl), and AgCl is collected on a glass microfiber filter and allowed to dry for ~1 hr. AgCl is reacted with CH_3I at 80 °C for 48 hours to produce CH_3Cl, the analyte measured in a gas-source mass spectrometer.

3.2.2 IRMS MEASUREMENT

Samples were measured by continuous flow using a ThermoElectron MAT 253 isotope ratio mass spectrometer (IRMS). A Pyrex tube containing the CH_3Cl sample was introduced into a stainless-steel extraction line that uses He as the carrier gas. Methyl chloride and excess methyl iodide are separated in a gas chromatography (GC) column and pure CH_3Cl is then transferred to the ion source. Samples are measured relative to a CH_3Cl reference gas. The MAT 253 is equipped with an additional Faraday cup for measurement of ^{37}Cl, allowing ^{35}Cl and ^{37}Cl to be measured at mass/charge ratios of ~50 and 52, respectively. Samples are standardized relative to Standard Mean Ocean Chloride (SMOC) water which by definition has a $\delta^{37}Cl$ value of 0‰. An internal rock standard from Elba, Italy ($\delta^{37}Cl$ = +1.3‰) and Carmel and Elba seawater ($\delta^{37}Cl$ = 0‰) are used to determine measurement precision. The rock standard is processed through all methods used for analysis of experimental products (specifically pyrohydrolysis); therefore, it is the best standard to ensure reproducibility of pyrohydrolysis procedures and IRMS measurement. Measurement precision based on long term reproducibility of an Elba rock standard is 0.23‰ (1σ).

3.3 X-RAY DIFFRACTION

Powder XRD scans of synthesis products were completed on a Bruker D8 Advance X-Ray Diffractometer at the University of Texas at Austin. The Bruker D8 Advance is equipped with a θ/θ goniometer and NaI dynamic scintillator detector with a variable divergence slit. A small quantity (~10 mg) of sample was top-loaded onto 2.5 cm zero-background quartz plates and distributed as a thin layer over a large area. Operation conditions were 40 kV and 35 mA. Samples were rotated continuously and diffraction patterns were recorded from 5-61° 2θ, with a step size of 0.018 ° and a count rate of 1 s

per step. The total scan time for 1 run was ~ 1 hr. Mineral phases were identified using the program EVA.

3.4 ELECTRON MICROPROBE

Electron-probe microanalysis (EPMA) measurements were made at the University of Texas at Austin on a JEOL 8200 instrument equipped with five wavelength-dispersive spectrometers. Samples were powdered, mixed with epoxy, and mounted in holes drilled into acrylic plastic disks. A final polish of 0.3 μm alumina grit was used and synthesis products were analyzed for elements Na, Mg, Al, Si, K, Ca, Fe, Ti, and Cl by wavelength-dispersive spectroscopy (WDS). Operating conditions employed a 1 μm beam size, 10 nA beam current and 15 keV accelerating voltage. All elements were measured for 30 s on peak and 15 s for both high and low background measurements. Cl was measured with crystal PETH for 100 s on peak, and for 15 s on high and low background measurements. Crystal PETH was used because it is a large-area crystal that intercepts a wider arc of the emitted x-ray signal and ultimately yields higher count rates than a normal-sized crystal. Primary standards were anorthite glass, orthoclase, Kakanui-hornblende, synthetic fayalite, Amelia-albite, ilmenite, and scapolite. Kakanui-hornblende and scapolite were used as secondary standards. Analysis of small samples required a minimum (ca. 1 μm) spot size, increasing the probability of volatile diffusion (Na and Cl). To check for diffusion of Cl, a scapolite standard was analyzed between samples. Based on totals, analyses exhibited negligible volatile diffusion. Analysis totals were typically low due to the beam-excitation volume being greater than the volume of sample grains. To eliminate analyses that suffered from low X-ray counts, analyses with oxide totals > 65 wt% and cation sums of 16 (± 0.3) apfu were taken as appropriate. To

correct Cl concentrations, samples with totals < 98 wt% were recast to a reasonable 98% total to correct for low element concentrations (e.g., Giblin et al., 1993).

Chapter 4: Results

4.1 SYNTHESIS PRODUCTS

4.1.1 XRD AND EPMA RESULTS

Twenty reconnaissance experiments were run prior to choosing a starting composition for fractionation experiments (experiments labeled HAST1-1 to HAST3-25). Exemplary reconnaissance experiments and experimental conditions for all runs used to determine Cl isotope fractionation (HAST3-26 and greater) are given in Table 2. Samples retrieved from the capsule were generally hard and compact. Only experiments that used a 1:1 fluid-rock ratio were noticeably soft. Synthesis products were scanned by XRD. If hydroxyl-bearing minerals were synthesized, the starting composition was altered (e.g., eliminating K from bulk composition to avoid mica stability). Non-amphibole minerals that contain structurally bound OH^- groups could incorporate Cl and contribute to Cl isotope partitioning. Stabilization of phases that are not Cl-bearing was not a concern. The starting composition chosen for Cl isotope fractionation experiments was $NaCa_2(Fe_4^{2+},Fe^{3+})(Al_2Si_6)O_{22}(OH,Cl)_2$ (HAST 3). This composition hosted sufficient Cl (~400-800 ppm) to warrant a meaningful isotopic measurement by IRMS using ~100 mg of powder and synthesis products were predominantly amphibole. Based on XRD analyses, samples synthesized at 700 °C and 0.2 GPa were composed of > 95% hastingsite (Fig. A5). The remaining material was Fe-oxides and pyroxene, which should not contribute to the bulk-sample and solution $\delta^{37}Cl$ values [Fe-oxides and pyroxene do not incorporate structural Cl and have neutral surfaces (Deer et al., 1966), eliminating potential ion-filtration-based fractionation.]

Average compositions of amphiboles analyzed by EPMA are given in Table 3. Amphiboles were classified according to the Leake et al. (1997) classification scheme for

calcic amphiboles ($Ca_B \geq 1.50$ and $(Na + K)_A \geq 0.5$). A scanning electron microscope (SEM) secondary electron image of products shows that amphibole products were small (5 μm to < 1 μm), making quantitative analyses challenging (e.g., Fig. 2). The Fe^{2+}/Fe^{3+} ratio was determined by using the procedure presented by J.C. Schumacher in the Leake et al. (1997) Appendix for determining the proportions of ferric to ferrous iron. Although determining meaningful Fe^{2+}/Fe^{3+} (or IV-Al proportions) from stoichiometry can lead to erroneous estimates, this was the best result that could be deduced from EPMA data, and can provide an approximation of the Fe^{2+}/Fe^{3+} ratio and site assignments for the purpose of naming the amphibole. EPMA data points of amphiboles synthesized in fractionation experiments plot within the hastingsite field ($^{IV}Al < Fe^{3+}$), denoting moderate Si apfu's (~6.0) and low $Mg/(Mg + Fe^{2+})$ ratios (Fig. 3). Average Cl concentrations of fractionation-experiment products were ~500 ppm, based on renormalization of totals to 98 wt%. The highest Cl concentrations (~7000 ppm) were seen in experiments that employed bulk composition HAST 1, specifically NaCl(s) in the starting composition; however, Cl heterogeneity in products was very large (1000-2000 ppm). Secondary phases stabilized varied from Fe-rich oxides to pyroxene based on EDS analyses. The stability of pyroxene was only seen in experiments with an F/R of 0.3 and 1.

4.1.2 SEM IMAGING OF SYNTHESIS PRODUCTS

SEM examination of synthesis products from fractionation experiments reveals nearly complete conversion of the charge to amphibole. Images of amphibole products show equigranular grain sizes (Fig. 2), typically ranging from 1 to 5 μm in length and ≤ 1 μm in width. Fig. 2B is a back-scattered electron (BSE) image that shows amphiboles are typically found as fine-grained dark elongate crystals. Amphiboles generally form long rectangular or diamond-cross shapes, and also large polycrystalline aggregates with

indistinguishable grain boundaries. Fe-oxides form as larger, more euhedral grains. Pyroxenes were also larger and more euhedral. Fe-oxides were brighter in BSE images because of the high concentration of Fe, whereas pyroxenes have about the same grey level as amphiboles. SEM images showed that pyroxene was only present in experiments run with fluid-rock ratios greater than 0.2, however, pyroxene is below the detection limit of XRD scans.

Table 2. Synthesis conditions and experimental products

Sample	P (MPa)	T (°C)	time (hr)	F/R†	Products and comments#
HAST 1-1*	200	700	70	No fluid	Amph, An, [Fay], [Hed]
HAST 1-2*	200	700	69	0.05	Amph, An, [Fay], [Hed]
HAST 2-3*	200	700	41	0.28	Amph, Phl
HAST 2-4§	375	800	19	0.16	Amph
HAST 2-21	200	700	73	0.27	Amph, Phl
HAST 2-22	200	700	73	0.28	Amph, Phl
HAST 3-23	200	700	75	0.25	Amph
HAST 3-26‡‡	200	700	172	0.20	Amph
HAST 3-27	200	700	120	0.20	Amph
HAST 3-28	200	700	76	0.21	Amph
HAST 3-29	200	700	169	0.19	Amph
HAST 3-30	200	700	122	0.21	Amph
HAST 3-31	200	700	121	0.20	Amph
HAST 3-32	200	700	168	0.19	Amph
HAST 3-33	200	700	73	0.20	Amph
HAST 3-35	200	700	336	0.30	Amph
HAST 3-36	200	700	336	0.30	Amph
HAST 3-37	200	700	336	0.30	Amph
HAST 3-38	200	700	341	0.30	Amph
HAST 3-39	200	700	341	0.29	Amph
HAST 3-43	200	700	168	0.20	Amph
HAST 3-44	200	700	121	0.18	Amph
HAST 3-47	200	700	161	1.00	Amph
HAST 3-48	200	700	185	0.99	Amph
HAST 3-49	200	700	528	0.20	Amph
HAST 3-40††	200	600	120	0.29	Glass, Amph
HAST 3-41	150	600	72	0.27	Glass, Amph
HAST 3-42	200	600	336	0.20	Glass, Amph

*Experiments done at Binghamton University with Cold-Seal Pressure Vessels

§Experiment done at Binghamton University with Internally-Heated Pressure Vessels at an fH_2 = 6 MPa

†Fluid to rock ratio (by mass)

#Phases are listed in the order of their abundance (approximated by inspection of X-ray pattern); phases indicated by [] are present at 5 wt% or less. Samples were dark green in color.

‡‡Conditions and synthesis products of runs that were used determine equilibrium Cl isotope fractionation.

††Amphibole synthesis attempts at 600 °C

Experiments above the solid line (HAST 1-1 to HAST 3-23) are preliminary synthesis experiments.

Abbreviations: Amph = amhibole, An = anorthite, Fay = fayalite, Hed = hedenbergite, Phl = phlogopite

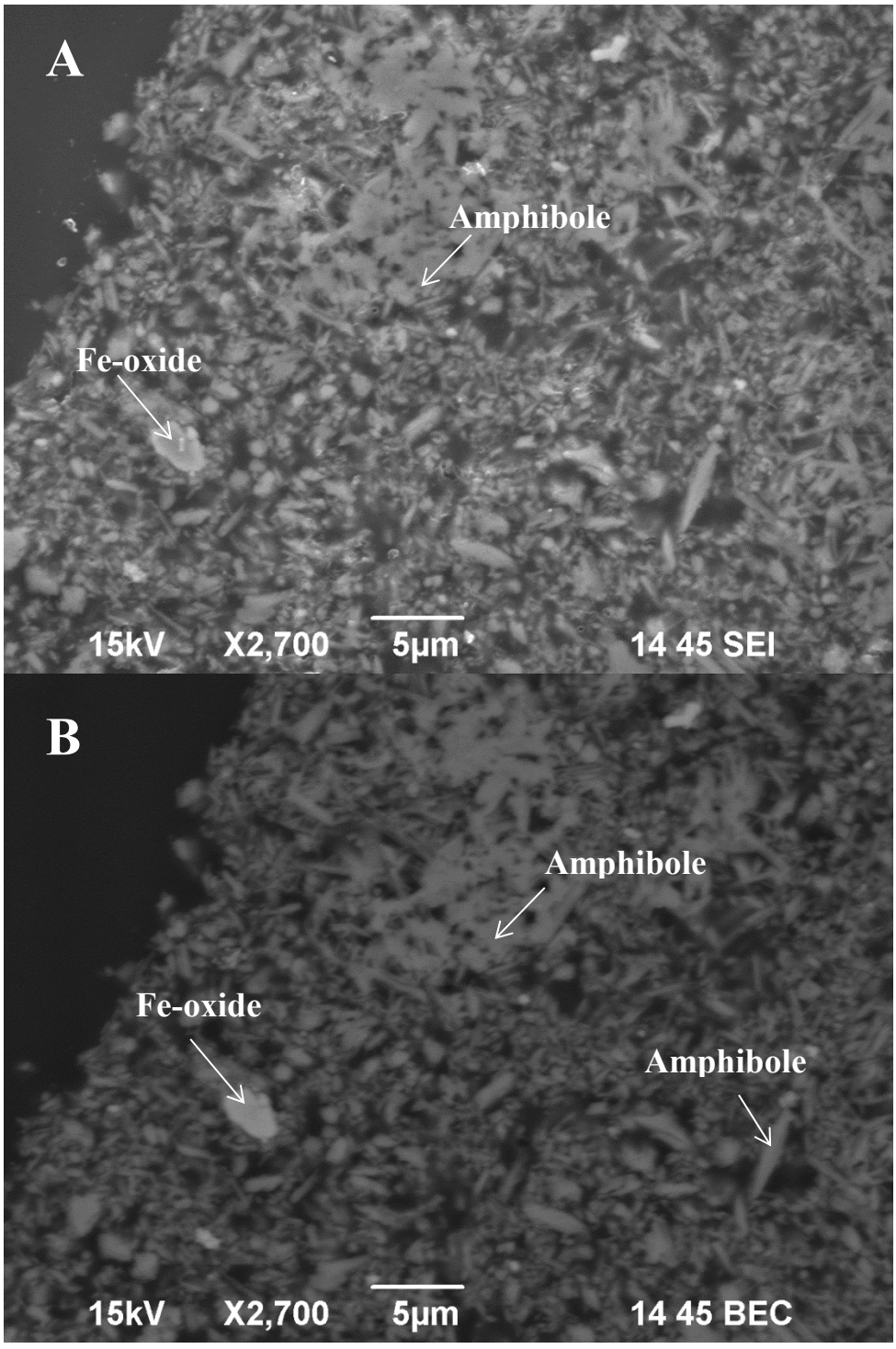

Figure 2. SEM images of synthesis products. A: Secondary electron image, B: Backscattered-electron composition image. Bright grains in the BSE Compo image are iron oxides; the remaining crystals are amphibole (hastingsite).

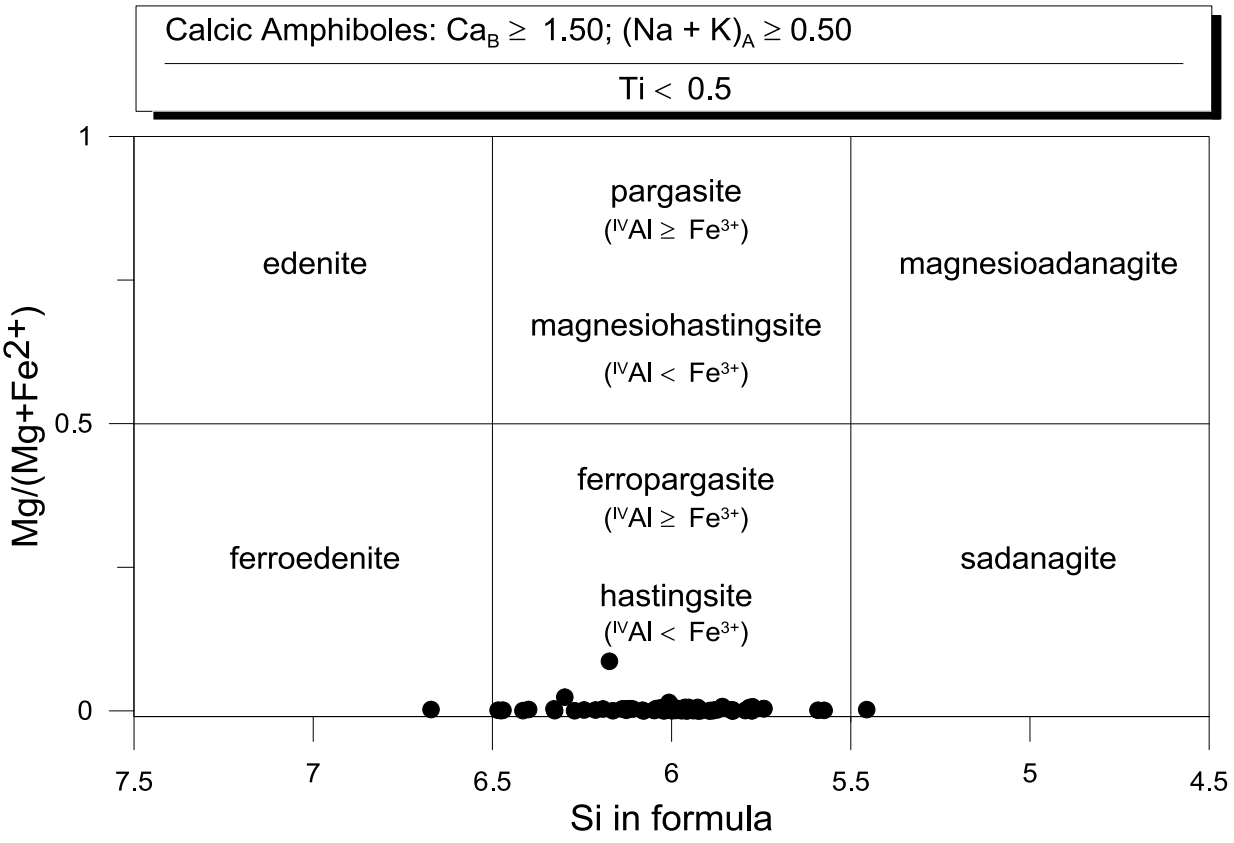

Figure 3. Classification scheme for calcic amphiboles. Each data point is a single electron-probe spot on multiple grains from experiments analyzed by EPMA. All synthetic amphiboles plot within the field of high-ferric-iron calcic amphiboles, those being hastingsite. Figure modified from Leake et al. (1997).

Table 3. Average compositions (wt%) of synthetic amphiboles

Sample	HAST 3-26	HAST 3-29	HAST 3-30	HAST 3-32	HAST 3-33	HAST 3-35	HAST 3-36	HAST 3-37	HAST 3-38	HAST 3-39
n#	2	4	9	9	10	16	6	11	7	8
SiO_2	32.69	32.66	34.65	33.00	33.00	35.84	31.17	32.24	34.11	34.19
Al_2O_3	8.21	10.86	12.28	10.03	10.03	12.08	9.53	9.58	10.06	10.88
FeO	27.82	29.83	32.90	31.28	31.28	34.06	29.15	30.17	32.40	33.59
MgO	0.02	0.05	0.01	0.01	0.01	0.09	0.28	0.02	0.07	0.00
CaO	10.64	10.73	10.52	9.89	9.89	10.29	8.86	9.25	9.91	9.98
Na_2O	2.72	3.10	3.68	3.22	3.22	3.61	3.09	3.27	3.19	3.61
K_2O	0.04	0.03	0.03	0.02	0.02	0.04	0.04	0.02	0.03	0.02
Cl	0.06	0.04	0.05	0.04	0.04	0.08	0.05	0.04	0.06	0.03
Total	82.18	87.31	94.13	87.50	87.50	96.10	82.17	84.58	89.83	92.31
Site assignments‡*†										
^{IV}Si	6.47	5.97	5.96	6.06	6.04	5.93	5.97	6.10	6.08	5.92
^{IV}Al	1.53	2.03	2.04	1.94	1.96	2.08	2.03	1.90	1.92	2.08
^{C}Al	0.39	-0.25	0.34	0.32	0.21	0.27	0.15	0.21	0.18	0.13
$^{C}Fe^{3+}$	0.00	0.49	0.66	0.70	0.70	0.98	1.05	0.80	0.83	1.00
$^{C}Fe^{2+}$	4.61	4.75	4.00	3.97	4.10	3.73	3.74	3.97	3.97	3.87
^{C}Mg	0.00	0.01	0.00	0.01	0.00	0.02	0.07	0.01	0.02	0.00
C(total)	5.00	5.00	5.00	5.00	5.00	5.00	5.00	5.00	5.00	5.00
^{B}Ca	2.26	2.57	2.00	1.85	1.94	1.82	1.80	1.89	1.89	1.86
^{B}Na	-0.26	-0.57	0.00	0.15	0.06	0.18	0.20	0.11	0.11	0.14
B(total)	2.00	2.00	2.00	2.00	2.00	2.00	2.00	2.00	2.00	2.00
^{A}Na	1.30	1.48	1.18	1.03	1.09	0.98	1.00	1.07	0.99	1.07
^{A}K	0.01	0.01	0.01	0.01	0.01	0.01	0.01	0.01	0.01	0.00
Cations	16.31	16.48	16.19	16.04	16.09	15.99	16.01	16.07	16.00	16.07

n denotes the number of individual of analyses

‡Mineral formula (apfu) is calculated on the basis of 22O + 2OH

*Site assignments are based on restricting only Ca and Na to the M4 site

†Amphibole sites are based on the general formula $A_{0\text{-}1}B_2C_5T_8O_{22}(OH)_2$ - $A_{0\text{-}1}M4_2(M1_2M2_2M3_1)_5T_8O_{22}(OH)_2$

4.2 FRACTIONATION EXPERIMENTS

Starting and final $\delta^{37}Cl$ values of solutions and samples are given in Table 4. Initial $\delta^{37}Cl$ values of the samples do not exist because starting reagents were not Cl-bearing. $\delta^{37}Cl$ values of the solutions were determined by measuring the Cl isotope composition of the fluid after the experiment using IRMS, following methods in section 3.2.1. Many authors have preferred to calculate final fluid δ values by mass balance, but determining $\delta^{37}Cl$ values of the final fluid by mass balance proved difficult for three reasons: (1) uncertainty in final solution Cl^- concentrations due to error in IC measurements; (2) error in Cl concentrations of amphiboles from EPMA analysis due to low X-ray counts; and (3) synthesis products were not 100% amphibole, leading to further uncertainty in calculations. Fractionation factors were therefore determined using the final $\delta^{37}Cl$ of the fluid measured by IRMS. Fractionation factors are given in Table 4.

Figure 4 displays final $\delta^{37}Cl$ values of amphiboles reacted with seawater and a high $\delta^{37}Cl$ solution plotted against time. Cl isotope values of amphiboles reacted with seawater display a 3-day $\delta^{37}Cl$ value of +0.62‰. At 5 days, $\delta^{37}Cl$ values decrease toward negative values of -0.25‰ and -1.29‰. After 7 days $\delta^{37}Cl$ values remained nearly constant with values of -0.07‰, -1.17‰, and -0.23‰. At 14 days, $\delta^{37}Cl$ values of ~+0.1‰ are reached (n = 2). Amphiboles reacted with a high $\delta^{37}Cl$ solution ($\delta^{37}Cl$ = +10.36‰) have a $\delta^{37}Cl$ value of +1.64‰ at 3 days. $\delta^{37}Cl$ values of the amphibole increase to +2.82‰ and +3.50‰ at 5 days, and decrease to +1.34‰ and +1.08‰ at 7 and 8 days, respectively. The average final $\delta^{37}Cl$ value at 14 days is +1.12‰ (n = 3). Short-duration experiments (e.g., 5 days) displayed poor reproducibility, whereas replicates of longer duration experiments show much better agreement. $10^3 ln\alpha_{amphibole\text{-}fluid}$ values showed behavior that is not consistent with $\delta^{37}Cl$ values of amphiboles.

Calculated $10^3 \ln\alpha_{amphibole\text{-}fluid}$ values show behavior that varies based on the fluid-rock ratio used in synthesis-reaction experiments (Fig. 5). Synthesis-reaction experiments between amphibole and a ^{37}Cl-enriched solution that used a low fluid-rock ratio of 0.2 monotonically approach calculated $10^3 \ln\alpha_{amphibole\text{-}fluid}$ values of amphibole reacted with seawater. Amphibole and high-$\delta^{37}Cl$-value solution experiments that employ higher fluid-rock ratios (0.3 - 1.0) never approach $10^3 \ln\alpha_{amphibole\text{-}fluid}$ values of seawater. $10^3 \ln\alpha_{amphibole\text{-}fluid}$ values for amphibole-seawater experiments are fairly consistent, independent of the fluid-rock ratio employed.

Table 4. Cl isotope data for amphibole-water fractionation experiments

Sample	P (MPa)	T (°C)	t (days)	Water (mg)	Oxides (mg)	F/R	Avg. [Cl]†	$\delta^{37}Cl_{water\text{-}intial}$	$\delta^{37}Cl_{amph\text{-}final}$	$\delta^{37}Cl_{water\text{-}final}$	$10^3 ln\alpha_{amph\text{-}water}$
HAST 3-28	200	700	3	27.6	134.5	0.21		0.00	0.62	-0.13	0.74
HAST 3-27	200	700	5	23.6	116.3	0.20		0.00	-0.25	0.05	-0.30
HAST 3-31	200	700	5	29.7	146.4	0.20		0.00	-1.29	1.57	-2.86
HAST 3-26	200	700	7	23.7	118.4	0.20	588	0.00	-0.07	0.01	-0.08
HAST 3-32	200	700	7	29.0	153.3	0.19	694	0.00	-1.17	2.10	-3.27
HAST 3-47	200	700	7	138.6	138.9	1.00		0.00	-0.23		
HAST 3-36	200	700	14	60.0	199.6	0.30	654	0.00	0.10	-0.02	0.12
HAST 3-38	200	700	14	54.9	181.1	0.30	655	0.00	0.13	0.34	-0.21
HAST 3-33	200	700	3	30.7	157.2	0.20	456	10.36	1.64	9.90	-8.21
HAST 3-30	200	700	5	21.8	105.2	0.21	521	10.36	2.82	2.92	-0.10
HAST 3-44	200	700	5	19.9	110.1	0.18		10.36	3.50		
HAST 3-29	200	700	7	20.5	110.7	0.19	414	10.36	1.34	0.91	0.43
HAST 3-43	200	700	7	27.3	140.0	0.20		10.36			
HAST 3-48	200	700	8	149.2	151.1	0.99		10.36	1.08	8.70	-7.58
HAST 3-35	200	700	14	56.6	189.5	0.30	808	10.36	1.19	2.38	-1.19
HAST 3-37	200	700	14	57.4	194.3	0.30	494	10.36	1.18	8.23	-7.02
HAST 3-39	200	700	14	52.5	179.2	0.29	392	10.36	0.98	9.06	-8.04
HAST 3-49	200	700	22	24.2	122.4	0.20					
HAST 3-41	150	600	3	20.0	73.5	0.27		0.00			
HAST 3-40	200	600	5	14.8	51.2	0.29		0.00			
HAST 3-42	200	600	14	22.7	111.9	0.20		0.00			

†Cl concentrations are corrected by recasting low EPMA totals to ~98wt% and are reported in ppm

Abbreviations: Amph = Amphibole

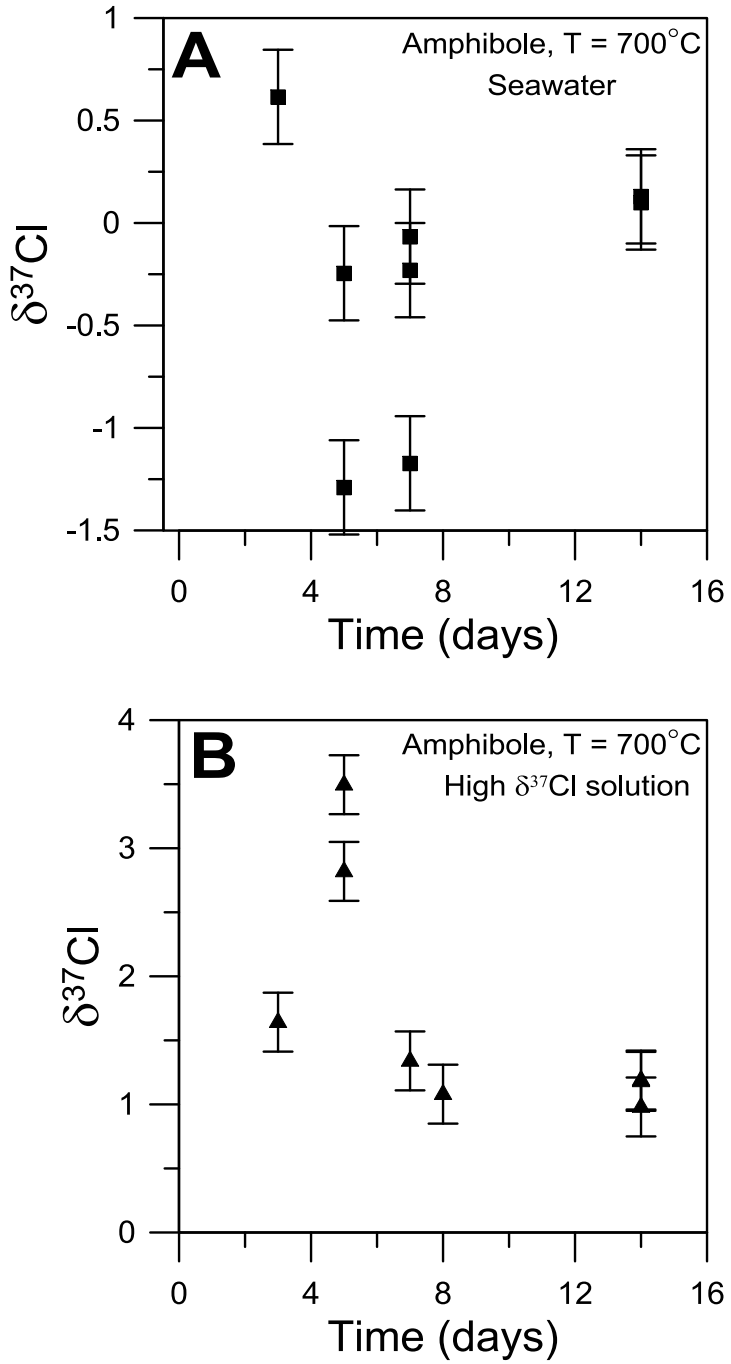

Figure 4. $\delta^{37}Cl$ values of hastingsite vs. time. A: $\delta^{37}Cl$ values of hastingsite reacted with seawater. B: $\delta^{37}Cl$ values of hastingsite reacted with a high $\delta^{37}Cl$ solution.

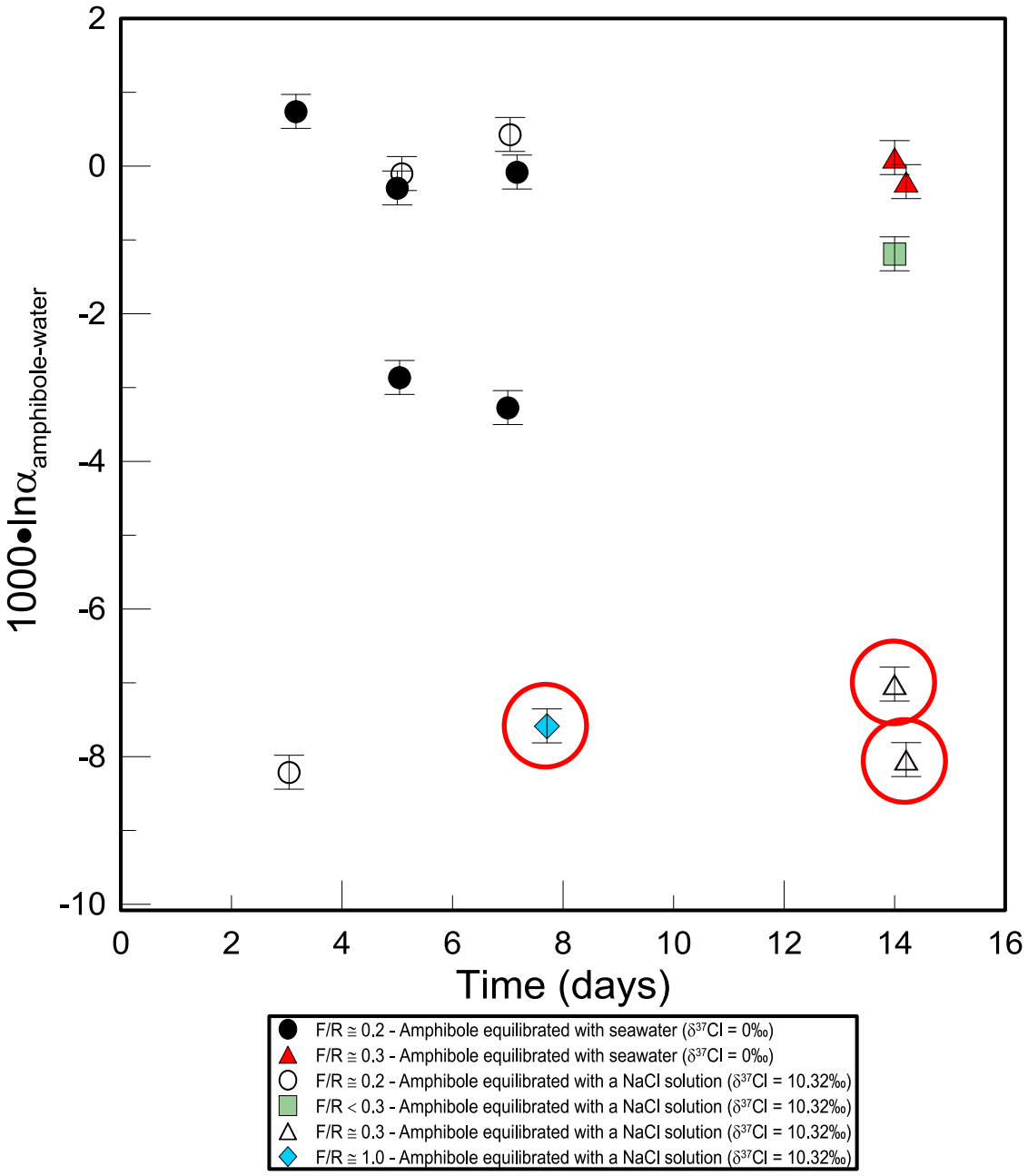

Figure 5. $10^3 ln\alpha_{hastingsite\text{-}fluid}$ *values of hastingsite-fluid pairs vs. time. Synthesis-reaction experiments between amphibole and a high-*$\delta^{37}Cl$ *solution that employ fluid-rock ratios greater than 0.2 do not approach* $10^3 ln\alpha_{amphibole\text{-}fluid}$ *values of amphibole reacted with seawater (encircled in red).*

Chapter 5: Discussion

5.1 Recommended fractionation factor

Experiments reacting amphibole with a high-$\delta^{37}Cl$ solution that employed a fluid-rock ratio of 0.3 or greater display $10^3ln\alpha_{amphibole\text{-}fluid}$ values that are not representative of equilibrium fractionation at 700 °C, based on unequal $10^3ln\alpha_{amphibole\text{-}fluid}$ values of amphibole reacted with a high-$\delta^{37}Cl$ solution and amphibole reacted with seawater. It is likely that experiments between amphibole and seawater do not show large variations in $10^3ln\alpha_{amphibole\text{-}fluid}$ values because the system was initially near its equilibrium $10^3ln\alpha_{amphibole\text{-}fluid}$ value. Experiments between amphibole and a high-$\delta^{37}Cl$ solution that employed a fluid-rock ratio of 0.2 reached fractionation factors of $10^3ln\alpha_{amphibole\text{-}fluid}$ = 0.43‰ within 7 days, values that seem reasonable in comparison to theoretical and empirical results described below. I therefore suggest that experiments employing fluid-rock ratios of 0.2 are more representative of equilibrium fractionation between an amphibole and a fluid. It is possible that high fluid-rock ratio experiments have undergone some incongruent dissolution, considering a fluid-rock of < 0.1 is sufficient to completely convert a charge to amphibole (Thomas, 1982). Mg isotope fractionation during dissolution has been well documented. Pearce et al. (2012) noted Mg isotope fractionation between magnesite and fluid, wherein the $\delta^{26}Mg_{fluid}$ value becomes 0.4‰ greater than the $\delta^{26}Mg_{solid}$ following dissolution of magnesite into the fluid. It is unlikely, however, that dissolution is occurring, considering that textural evidence of dissolution is not present, and dissolution would require understauration of the fluid after crystallization of amphibole, an unlikely scenario. Therefore the reason for lack of progression of $10^3ln\alpha_{amphibole\text{-}fluid}$ values for amphibole/high-$\delta^{37}Cl$-solution reactions towards $10^3ln\alpha_{amphibole\text{-}fluid}$ values of amphibole-seawater experiments is unknown.

By using a least-squares regression, best-fit lines were placed through the data, that is, amphibole-high-δ^{37}Cl-solution experiments that employed a fluid-rock ratio of 0.2 (n = 3), and all amphibole-seawater reactions (n = 5) excluding outliers HAST 3-31 and HAST 3-32. $10^3\ln\alpha_{amphibole\text{-}fluid}$ values for amphibole/seawater experiments were best fit by a second-order exponential decay function equation and those for amphibole/high-δ^{37}Cl-solutions were best-fit by an exponential associate equation (Fig. 6, Table B4). The extrapolations to the steady-state $10^3\ln\alpha_{amphibole\text{-}fluid}$ values are within IRMS measurement error (2σ) of 14 day $10^3\ln\alpha_{amphibole\text{-}seawater}$ values. $10^3\ln\alpha_{amphibole\text{-}fluid}$ values are used for calculating the final fractionation factor, not extrapolated values from best-fit lines. Using the average of 7 and 14 day $10^3\ln\alpha_{amphibole\text{-}seawater}$ values [$10^3\ln\alpha_{amphibole\text{-}seawater}$ = -0.06‰ (n = 3)], and the $10^3\ln\alpha_{amphibole\text{-}high\delta}$ 7 day value [$10^3\ln\alpha_{amphibole\text{-}high\delta}$ = 0.43‰ (n = 1)], a final fractionation of 0.19‰ ± 0.23‰ is calculated.

Experiments run for 3-5 days possibly suffer from kinetic isotope fractionation. If the fractionation is as small as determined above, δ^{37}Cl values of hastingsite should monotonically approach the δ^{37}Cl value of the corresponding fluid over time, whereas hastingsite in this study shows deviation from monotonic approach towards the fluid Cl isotope value. The process responsible for kinetic fractionation is more difficult to discern. Three-day δ^{37}Cl values of hastingsite reacted with seawater can be explained by preferential partitioning of ^{37}Cl into hastingsite during initial precipitation. Faster diffusion of ^{35}Cl from the fluid to the amphibole O3 site can explain the decrease in δ^{37}Cl values at 5 days; however, the same explanation does not hold for amphiboles reacted with a high-δ^{37}Cl solution. Hastingsite reacted with a high-δ^{37}Cl solution showed an increase in δ^{37}Cl values from 3 to 5 days, in contrast to hastingsite reacted with seawater. Hastingsite Cl isotope values monotonically approach the δ^{37}Cl value of the fluid (δ^{37}Cl = +10.36‰), which indicates that kinetic fractionation is negligible. From 7 to 14 days

however, $\delta^{37}Cl$ values decrease, in disagreement with monotonic approach towards the fluid Cl isotope value. It is not uncommon to notice that experiments "overshoot" equilibrium $10^3 ln\alpha_{mineral\text{-}fluid}$ values (e.g. Fig. A2, Saccocia et al., 2009).

Several explanations have been proposed for causes of kinetic isotope fractionation in experiments that involve synthesis of a single phase: (1) isotope fractionation following dissolution or precipitation during transition to equilibrium temperatures (e.g. Brantley et al., 2004; Wiederhold et al., 2006; Kiczka et al., 2010; Pearce et al., 2012); (2) Ostwald-ripening recrystallization (Matthews et al., 1983b; Matthews et al., 1983a); and (3) isotopic fractionation due to different diffusion rates of isotopes of an element. Currently the cause for kinetic fractionation in my experiments is unknown due to limited calibrations of Cl isotope fractionation during any of the processes mentioned above.

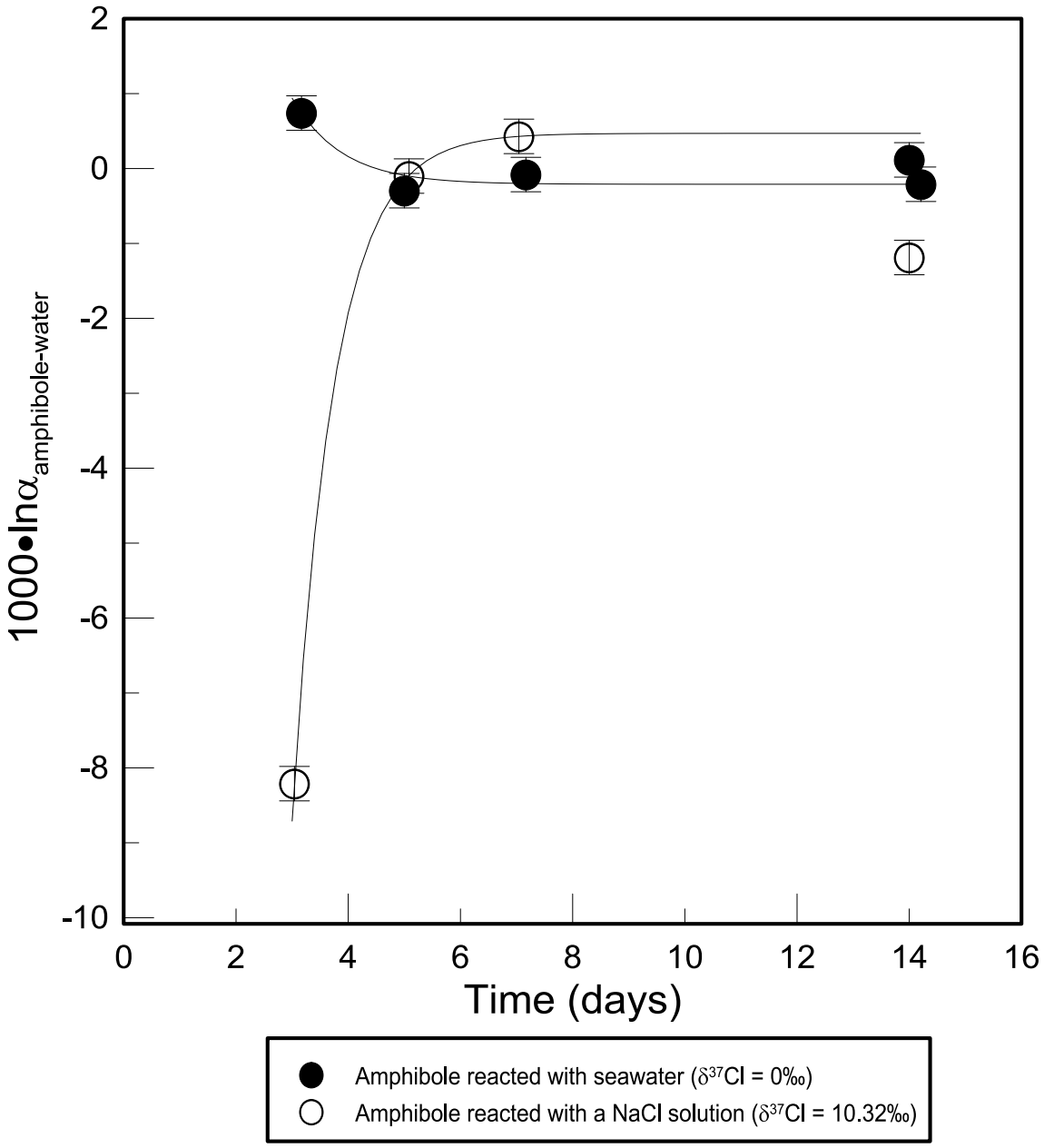

Figure 6. $10^3 ln\alpha_{amphibole\text{-}fluid}$ values of amphibole-fluid pairs vs. time. $10^3 ln\alpha_{amphibole\text{-}fluid}$ values of amphibole reacted with a ^{37}Cl enriched solution (F/R = 0.2) show monotonic approach toward equilibrium fractionation.

5.2 COMPARISON TO THEORETICAL RESULTS

Reduced partition function ratios have been calculated for $FeCl_2$, $MnCl_2$, and NaCl at 0 °C, 25 °C, 100 °C and 300 °C (Schauble et al., 2003). $FeCl_2$ is used as an analogue for amphiboles and $MnCl_2$ provides a validity test of $FeCl_2$ results, because it is much better studied spectroscopically. Results suggest that at 25 °C, $FeCl_2$ is ~2-3.5‰ heavier than NaCl (Fig. A6). Although reduced partition function ratios at temperatures greater than 300 °C have not been calculated, a linear extrapolation based on the given data estimates that minerals in which Cl^- is bonded to divalent cations, such as amphiboles and micas, have $\delta^{37}Cl$ values ~0.25‰ greater than coexisting NaCl-dominated brines at 700 °C. The calculated fractionation between amphibole and water from this study suggests that amphiboles have $\delta^{37}Cl$ values ~0.19‰ greater than coexisting fluid at 700 °C. I note that caution should be used with large extrapolations because not all isotopic systems follow consistent behavior (e.g. solid enriched in heavy isotope relative to a fluid) and previous studies have "crossovers" in isotope fractionation dependent on the temperature (e.g., fluid becomes enriched in the heavy isotope relative to the solid at high temperature), especially in hydrous silicates (Fig. A4, O'Neil and Taylor, 1969; Bottinga and Javoy, 1973; Matthews et al., 1983a; Zheng, 1993).

5.3 COMPARISON TO EMPIRICAL RESULTS

Two studies have measured Cl isotope values of AOC samples (Barnes and Cisneros, 2012; Bonifacie et al., 2007a). Barnes and Cisneros (2012) found that AOC rocks have $\delta^{37}Cl$ values that range from -1.4 to +1.8‰. AOC rocks dominated by amphibole have positive $\delta^{37}Cl$ values (> +0.5‰); however, those predominantly consisting of clay minerals have negative to near-zero $\delta^{37}Cl$ values. Altered gabbros have average $\delta^{37}Cl$ values of 0.6 ± 0.6‰, whereas extrusive lavas and sheeted dikes (basalts) have average Cl isotope compositions of 0.0 ± 0.6‰ and +0.1 ± 0.3‰, respectively.

Experimental results presented here are therefore consistent with empirical observations by Barnes and Cisneros (2012), wherein ^{37}Cl is preferentially partitioned into amphibole relative to the coexisting fluid. AOC samples display higher $\delta^{37}Cl$ values than predicted from my partitioning experiments, but hydrothermal alteration prevailed at lower temperatures than 700 °C, which should lead to larger magnitudes of Cl isotope fractionation between amphibole and fluid. The results are in disagreement with an earlier study that analyzed AOC samples from the East Pacific Rise, and measured $\delta^{37}Cl$ values ranging from -1.6 to -0.8‰ (n = 4) (Bonifacie et al., 2007). Mineralogy of the samples is not presented in the Bonifacie et al. (2007) study; therefore, it is difficult to discern whether differences in range of Cl isotope values are due to differences in mineralogy or measurement technique. It is believed that differences in measurement methods (continuous flow vs dual-inlet) have led to discrepancy of Cl isotope values of silicate rocks with low Cl concentrations, specifically the Cl isotope composition of the mantle (Sharp et al., 2007; Bonifacie et al., 2008). Constraining the reason for difference in $\delta^{37}Cl$ values is difficult, but, based on the fractionation factor $10^3 ln\alpha_{amphibole\text{-}fluid}$ = 0.19‰, I suggest that AOC rocks containing amphiboles should preferentially partition ^{37}Cl into amphibole relative to seawater.

Chapter 6: Conclusions

Chlorine isotope fractionation between an amphibole and fluid has been determined at 700 °C and 0.2 GPa using synthesis-reaction experiments. Isotope exchange between pargasite and fluid was kinetically inhibited at 600-800 °C and 50-100 MPa, likely due to the lack of extensive recrystallization and slow volume diffusion. Hastingsite was synthesized from an oxide mixture at 700 °C and 0.2 GPa, approximately around the wüstite-magnetite buffer, in the presence of either seawater or ^{37}Cl-enriched water, then allowed to react for varying lengths of time. Based on these synthesis-reaction experiments, the fractionation between amphibole and a NaCl-bearing solution at 700 °C can be approximated by $10^3\ln\alpha_{amphibole\text{-}fluid} = 0.19‰ \pm 0.23‰$. These results are consistent with Cl isotope behavior in hydrothermally altered gabbros: amphibole is the dominant Cl host phase and gabbros display δ^{37}Cl values averaging +0.6‰, implying preferential partitioning of ^{37}Cl into amphibole interacting with seawater (Barnes and Cisneros, 2012). The measured fractionation factor is also in good agreement with a linear extrapolation of theoretical calculations determined at lower temperatures, estimating an enrichment of ~0.25‰ in amphibole relative to coexisting NaCl solutions at 700 °C (Schauble et al., 2003).

Appendix: Figures

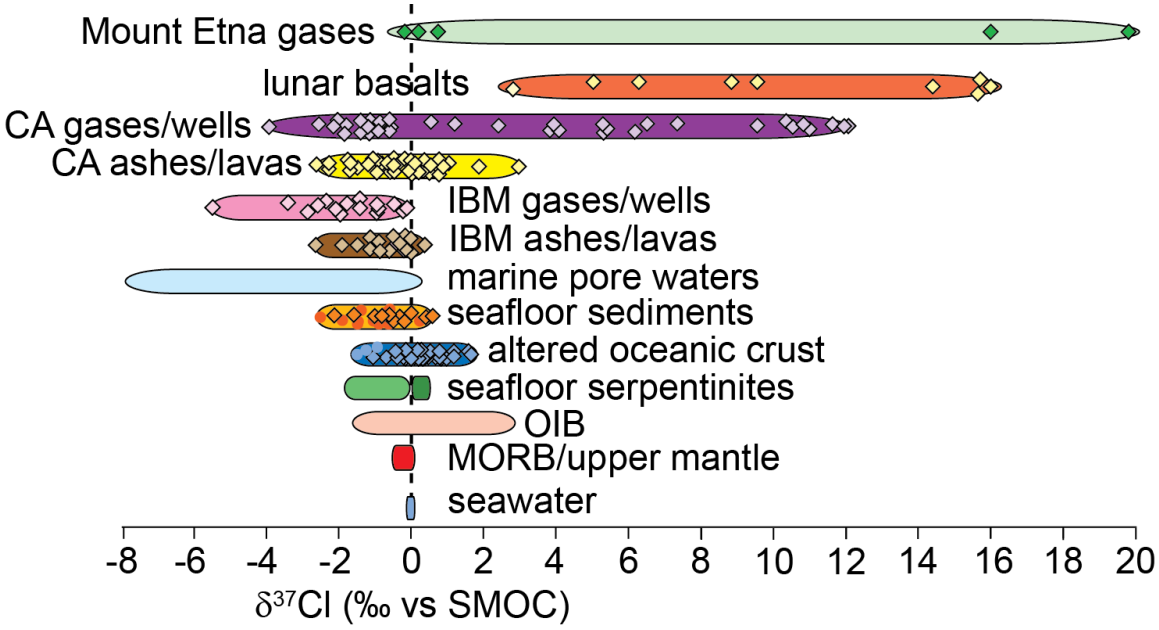

Figure A1: Cl isotope variation of terrestrial samples. $\delta^{37}Cl$ values are referenced from the following literature: Mount Etna gases (Italy) (Rizzo et al., 2013), lunar basalts (Sharp et al., 2010b), Central America (CA) gases/wells (Sharp et al., 2010a), Central America (CA) ashes/lavas (Barnes et al., 2009a), Izu-Bonin Mariana gases/wells and ashes/lavas(Barnes et al., 2008), marine pore waters (Spivack et al., 2002; Godon et al., 2004; Bonifacie et al., 2007b), seafloor sediments (Barnes et al., 2008), altered oceanic crust (Bonifacie et al., 2007a; Barnes and Cisneros, 2012), seafloor serpentinites (Barnes et al., 2006a; Bonifacie et al., 2008a), Ocean-island basalts (OIB) (John et al., 2011), Mid-Ocean Ridge basalts (MORB) (Sharp et al., 2007; Bonifacie et al., 2008b; Layne et al., 2009). Size of the symbol indicates the standard deviation of the measurement.

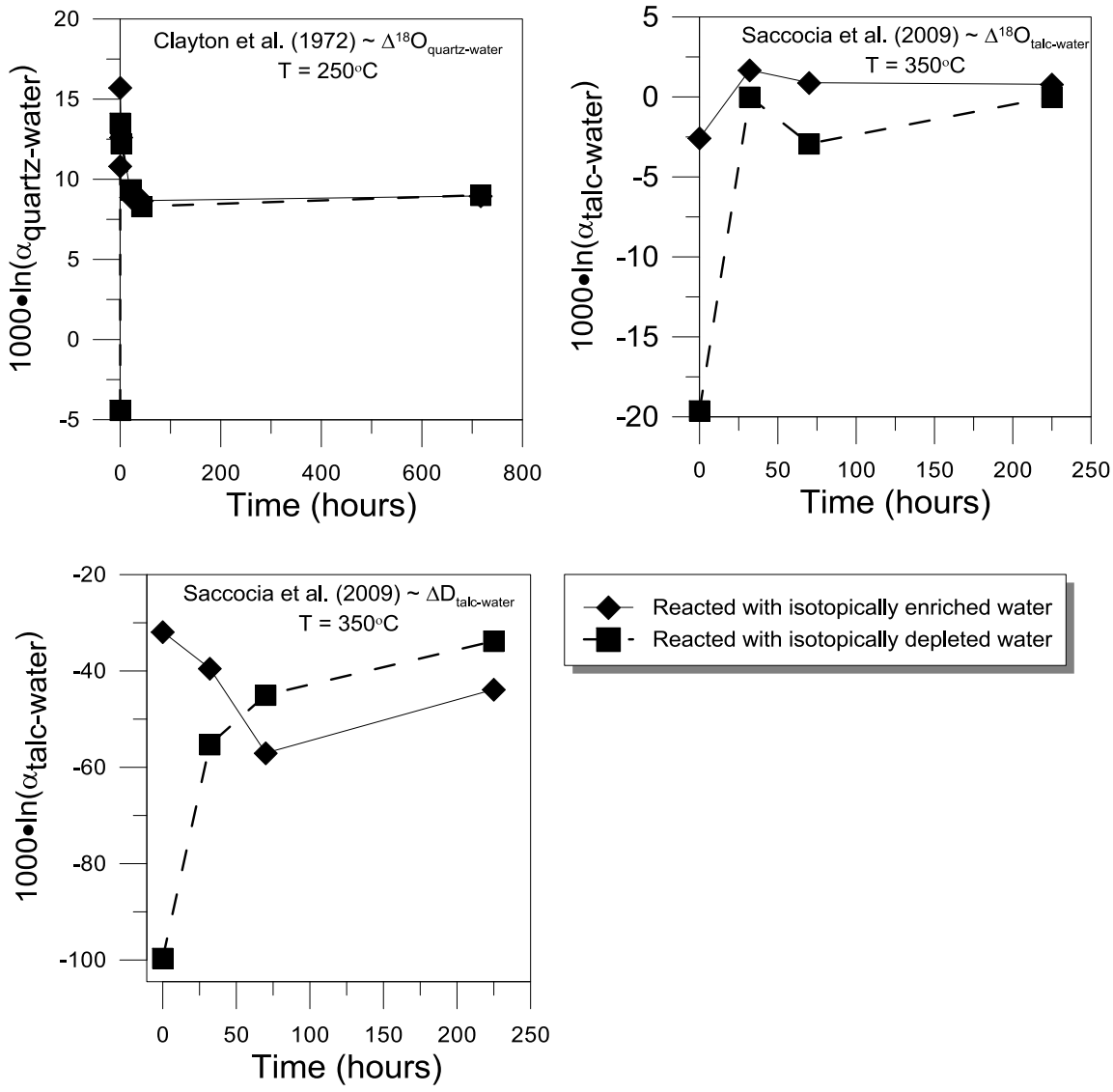

Figure A2. $10^3 ln\alpha_{mineral\text{-}water}$ values vs time for synthesis reaction experiments. After time t=0, $10^3 ln\alpha_{mineral\text{-}water}$ values are the same for $^{18}O/^{16}O$ and D/H measurements regardless of the starting isotopic composition of the solution (modified from Clayton et al., 1972; Saccocia et al., 2009).

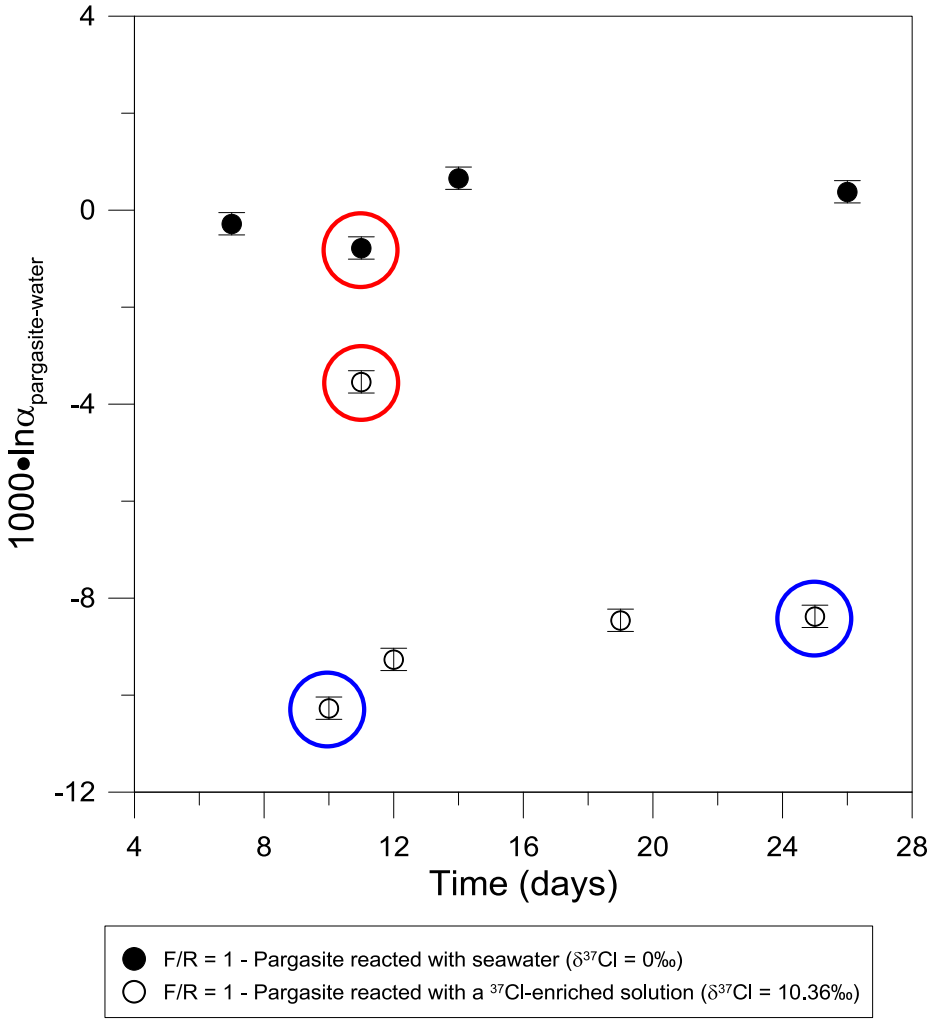

Fig. A3. $10^3 ln\alpha_{pargasite\text{-}water}$ values of pargasite-water reaction experiments vs. time. Cl isotope exchange rates were slow, even at high temperatures. Data points not encircled represent experiments run at 600 °C and 50 MPa. Reactions at 750 °C and 100 MPa (encircled in red) showed anomalously fast rates of isotope exchange. Experiments run at 800 °C and 100 MPa (encircled in blue) did not approach equal $10^3 ln\alpha_{pargasite\text{-}water}$ values for pargasite reacted with seawater and a ^{37}Cl-enriched solution, a concerning result considering exchange rates should increase at higher temperatures. The reason for large changes in $10^3 ln\alpha_{pargasite\text{-}water}$ values at 750 °C is therefore unknown.

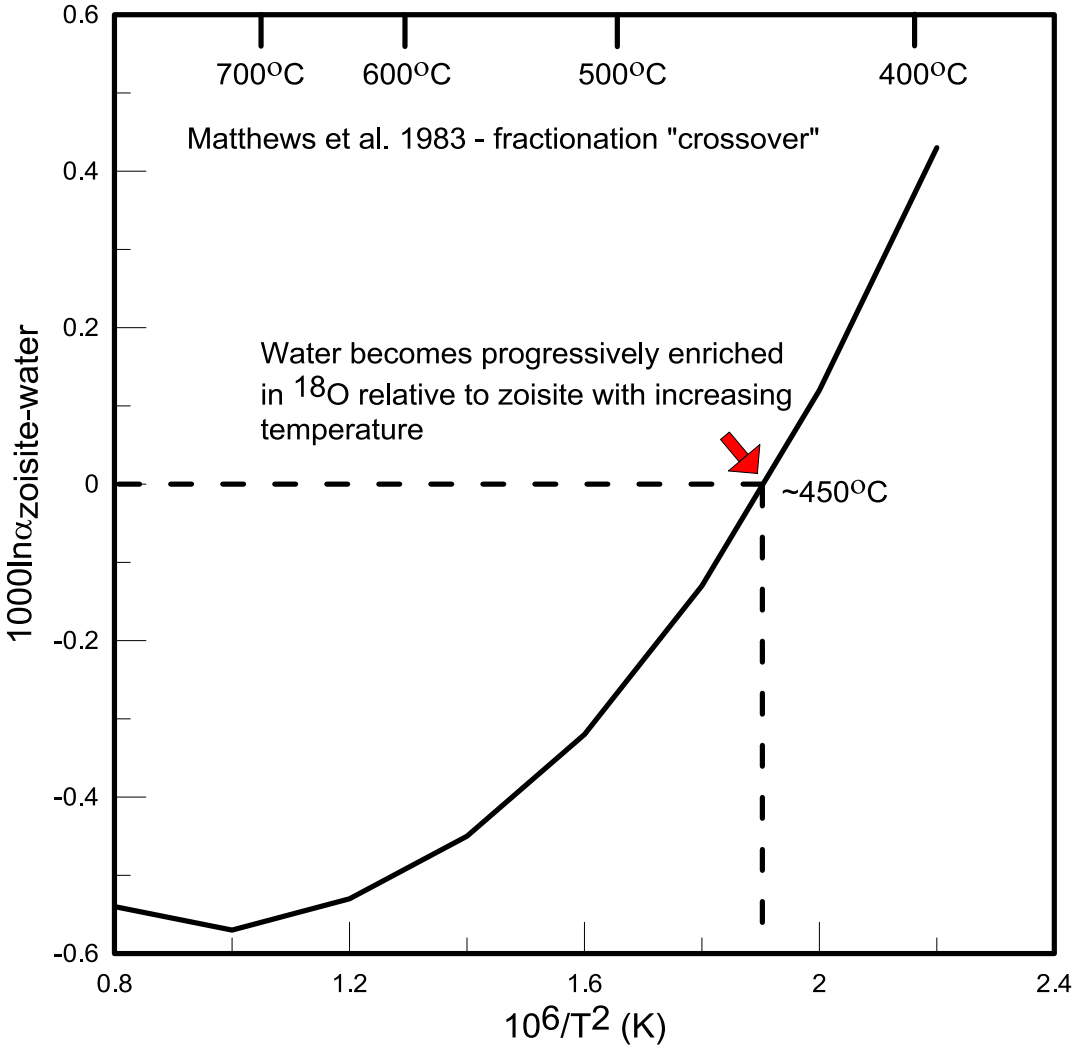

Figure A4. $10^3 ln\alpha_{zoisite\text{-}water}$ vs temperature. Experimental results display a crossover in fractionation at ~450 °C wherein water becomes progressively enriched in ^{18}O relative to zoisite with increasing temperature (modified from Matthews et al., 1983b).

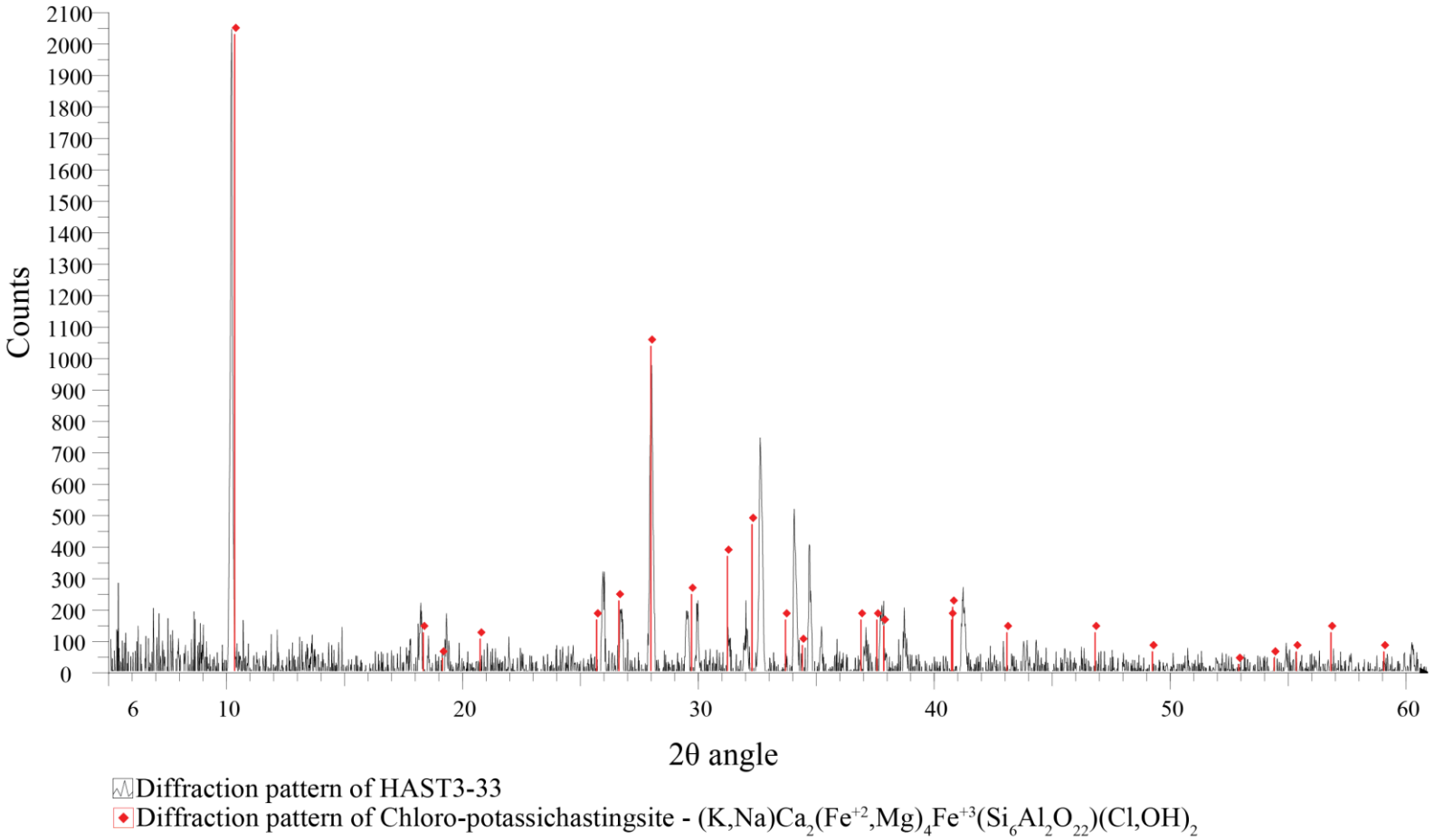

Figure A5. X-ray diffraction pattern of hastingsite (HAST3-33) is shown in black. Peaks in red represent characteristic 2θ peaks and intensities of a hastingsite. All hastingsite synthesized showed the same diffraction pattern. No noteworthy difference in 2θ peaks was observed in experiments with different fluid-rock ratios.

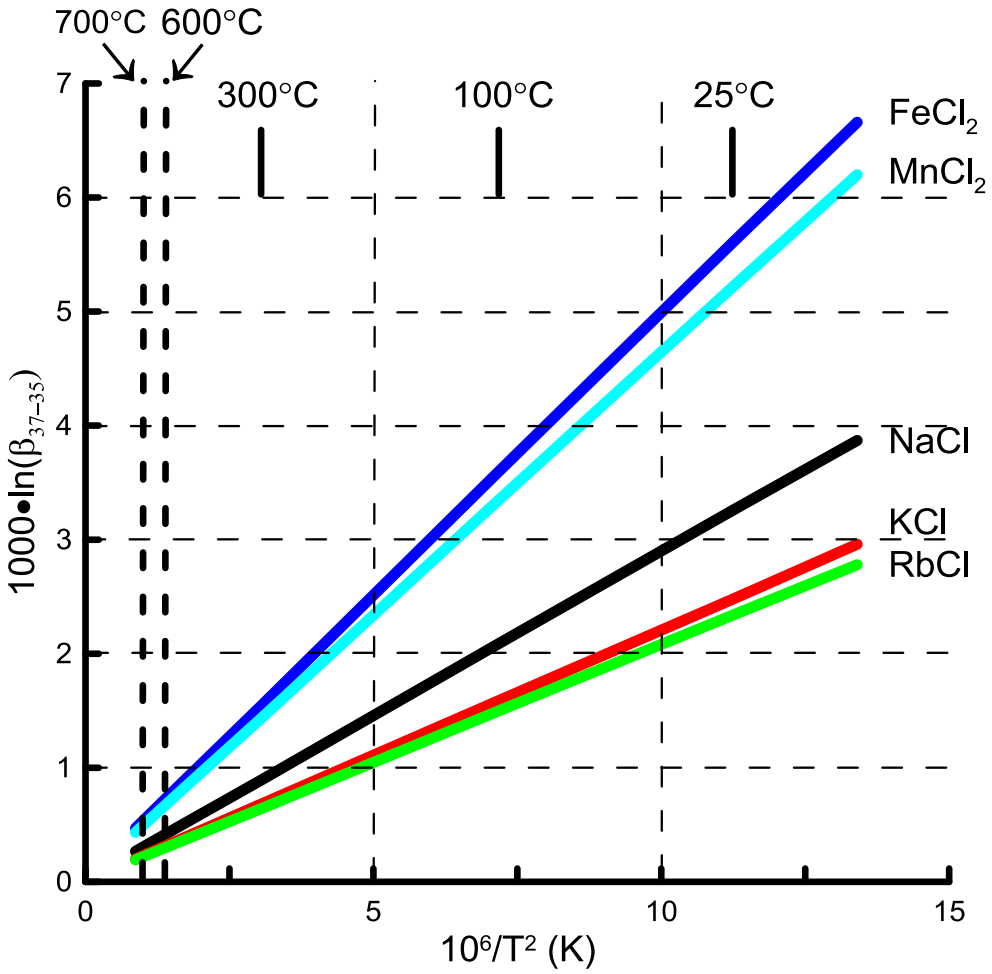

Figure A6. Reduced partition function ratios for alkali-chloride salts. Extrapolation of reduced partition function ratios demonstrates that $FeCl_2$ is enriched in ^{37}Cl by ~0.25‰ relative to NaCl-dominated brine at 700 °C. I note that reduced partition function ratios have not been determined at 700 °C, the data shown above is merely an extrapolation of data at 0 °C, 25 °C, 100 °C, and 300 °C (modified from Schauble et al., 2003).

Appendix: Tables

Table B1. Electron mircroprobe analysis (wt%) of standards

Sample†	Na_2O	MgO	Al_2O_3	SiO_2	Cl	K_2O	CaO	FeO	TiO_2	Total
Kakanui Hbl-1	2.51	12.75	14.02	39.87	0.03	1.94	9.98	10.46	4.59	96.13
	2.41	12.76	14.05	39.79	0.02	1.98	10.01	10.79	4.52	96.33
	2.54	13.00	13.97	39.70	0.02	2.00	10.01	10.33	4.81	96.37
Kakanui Hbl-2	2.53	12.71	13.90	39.74	0.02	1.98	9.94	10.28	4.74	95.83
	2.45	12.99	14.24	39.70	0.02	1.98	10.15	10.42	5.20	97.15
Kakanui Hbl-3	2.59	12.47	14.02	40.00	0.03	1.99	9.84	10.67	4.52	96.13
	2.57	12.80	14.10	39.88	0.03	1.98	10.04	10.50	4.29	96.19
	2.51	12.61	13.97	39.92	0.02	1.99	10.01	10.35	4.36	95.74
Kakanui Hbl-4	2.42	12.38	13.97	39.60	0.02	1.99	10.01	10.02	4.77	95.18
	2.35	12.38	13.76	39.08	0.02	1.97	9.99	10.27	4.95	94.77
Kakanui Hbl-5	2.43	12.65	14.01	39.89	0.03	2.00	9.96	10.47	4.35	95.78
	2.33	12.81	14.08	39.64	0.02	1.94	10.15	10.24	4.81	96.02
	2.42	12.59	14.07	39.69	0.03	1.97	10.08	10.42	4.81	96.07
	2.40	12.84	14.10	39.78	0.03	2.03	10.11	10.45	4.67	96.42
	2.42	12.46	14.26	40.02	0.03	1.96	9.98	10.52	4.64	96.29
Kakanui Hbl-6	2.42	12.62	14.17	40.05	0.02	2.02	10.06	10.62	4.75	96.72
	2.39	12.64	13.98	40.19	0.02	2.00	10.10	10.46	4.85	96.64
	2.62	12.67	14.12	39.97	0.02	2.02	10.10	10.40	5.21	97.15
	2.50	12.46	14.22	40.32	0.02	2.00	9.97	11.22	4.65	97.36
	2.56	12.56	14.02	40.11	0.02	1.97	9.98	10.84	5.07	97.13
Kakanui Hbl-7	2.58	12.98	14.23	40.14	0.02	1.95	9.86	10.38	4.58	96.73
	2.53	13.15	14.38	40.45	0.02	1.93	9.99	10.86	4.43	97.74
	2.62	13.05	14.18	40.30	0.02	1.95	9.89	10.42	4.53	96.96
	2.60	13.15	14.19	40.25	0.02	1.93	9.95	10.12	4.86	97.08
	2.48	13.27	14.11	40.47	0.02	1.96	9.93	10.48	4.43	97.15
Kakanui Hbl-8	2.43	12.91	14.28	40.35	0.02	2.01	10.02	10.49	4.72	97.24
	2.47	12.74	14.25	40.20	0.02	1.92	10.03	10.43	4.63	96.69
	2.46	12.80	14.22	40.25	0.02	2.01	10.11	10.68	5.10	97.65
	2.41	13.09	14.32	40.60	0.02	1.97	9.96	10.81	4.87	98.05
	2.58	12.85	14.19	40.32	0.02	1.94	9.81	10.82	4.49	97.00
Average	**2.48**	**12.77**	**14.11**	**40.01**	**0.02**	**1.98**	**10.00**	**10.51**	**4.71**	**96.59**
Kakanui Hbl‡	*2.60*	*12.80*	*14.90*	*40.37*	*0.00*	*2.05*	*10.30*	*10.92*	*4.72*	*98.66*
Std. Dev. (1σ)*	**0.08**	**0.24**	**0.14**	**0.32**	**0.00**	**0.03**	**0.09**	**0.25**	**0.24**	**0.74**
Std. Err. (1σ)**	**0.02**	**0.04**	**0.03**	**0.06**	**0.00**	**0.01**	**0.02**	**0.05**	**0.04**	**0.14**

†Run completed 3-26-13, ‡Recommended values for Kakanui Hbl standard

*Standard Deviation, **Standard Error, Abbreviations: Hbl = hornblende

Table B2. Electron mircroprobe analysis (wt%) of standards

Sample†	Na_2O	MgO	Al_2O_3	SiO_2	Cl	K_2O	CaO	FeO	TiO_2	Total
Kakanui Hbl-1	2.63	12.59	14.32	40.42	0.02	2.03	10.20	11.11	4.51	97.83
	2.74	11.79	14.48	40.48	0.03	2.09	9.79	11.60	4.92	97.91
	2.47	12.48	14.32	40.35	0.02	2.08	10.20	10.88	4.68	97.48
	2.54	12.67	14.35	40.29	0.02	2.07	10.05	11.36	5.13	98.48
Kakanui Hbl-2	2.69	12.37	14.43	40.13	0.02	2.03	10.03	11.24	4.65	97.60
	2.77	12.56	14.32	40.12	0.03	2.09	10.10	10.68	4.89	97.55
	2.56	12.56	14.37	40.28	0.02	2.03	10.14	11.50	4.86	98.33
Kakanui Hbl-3	2.69	12.55	14.15	39.43	0.02	2.04	10.07	11.08	4.84	96.87
	2.69	12.78	14.26	39.47	0.02	2.01	10.01	11.19	4.59	97.01
	2.79	12.89	14.35	39.55	0.03	2.04	9.98	10.88	4.83	97.35
Kakanui Hbl-4	2.57	12.30	14.10	39.54	0.03	2.11	10.11	11.12	4.70	96.58
	2.58	12.25	14.01	39.39	0.02	2.05	10.11	11.32	4.72	96.45
	2.59	12.46	14.05	39.34	0.02	2.06	10.22	10.85	4.97	96.56
	2.54	12.34	13.98	39.18	0.03	2.06	10.15	10.94	4.52	95.74
	2.50	12.29	14.02	39.33	0.02	2.03	10.15	10.74	4.91	96.00
Average	**2.62**	**12.46**	**14.23**	**39.82**	**0.02**	**2.05**	**10.09**	**11.10**	**4.78**	**97.18**
Kakanui Hbl‡	*2.60*	*12.80*	*14.90*	*40.37*	*0.00*	*2.05*	*10.30*	*10.92*	*4.72*	*98.66*
Std. Dev. (1σ)*	**0.10**	**0.26**	**0.17**	**0.48**	**0.00**	**0.03**	**0.11**	**0.27**	**0.18**	**0.81**
Std. Err. (1σ)**	**0.03**	**0.07**	**0.04**	**0.12**	**0.00**	**0.01**	**0.03**	**0.07**	**0.05**	**0.21**
Brazil Scp-1	5.40	0.01	25.29	49.85	1.43	0.88	13.55	0.11	0.01	96.52
	5.37	-0.02	25.27	49.90	1.44	0.86	13.51	0.11	-0.01	96.43
	4.09	0.00	25.71	50.72	1.46	0.79	13.17	0.13	0.04	96.10
	5.53	0.01	25.45	49.64	1.43	0.89	13.47	0.07	-0.01	96.49
Brazil Scp-2	5.33	0.00	24.99	48.67	1.41	0.84	13.48	0.07	0.04	94.84
	5.34	0.02	25.21	48.76	1.45	0.87	13.47	0.12	0.00	95.25
	5.59	0.00	25.29	48.87	1.44	0.88	13.46	0.10	0.03	95.67
	5.63	-0.01	25.15	48.72	1.43	0.88	13.47	0.09	0.01	95.37
Brazil Scp-3	5.45	0.01	25.03	48.57	1.43	0.85	13.48	0.12	0.01	94.95
	5.57	-0.01	24.88	48.78	1.45	0.85	13.25	0.08	0.00	94.85
	5.37	0.02	24.80	49.08	1.44	0.88	13.46	0.07	0.01	95.15
Average	**5.33**	**0.00**	**25.19**	**49.23**	**1.44**	**0.86**	**13.43**	**0.10**	**0.01**	**95.60**
Brazil Scp§	*5.26*	*0*	*25.05*	*49.78*	*1.43*	*0.94*	*13.58*	*0.17*	*0*	*96.21*
Std. Dev. (1σ)*	**0.43**	**0.01**	**0.26**	**0.69**	**0.01**	**0.03**	**0.12**	**0.02**	**0.02**	**0.67**
Std. Err. (1σ)**	**0.13**	**0.00**	**0.08**	**0.21**	**0.00**	**0.01**	**0.03**	**0.01**	**0.01**	**0.20**

†Run completed 4-7-13, ‡Recommended values for Kakanui Hbl std., §Recommended values for Brazil Scp std.
*Standard Deviation, **Standard Error, Abbreviations: Hbl = hornblende, Scp = scapolite

Table B3. Cl isotope data for pargasite-water fractionation experiments

Sample	P (MPa)	T (°C)	t (days)	F/R*	Avg. [Cl]†	$\delta^{37}Cl_{water\text{-}intial}$	$\delta^{37}Cl_{prg\text{-}inital}$	$\delta^{37}Cl_{water\text{-}final}$	$\delta^{37}Cl_{prg\text{-}final}$	$10^3 ln\alpha_{prg\text{-}water}$
G-785	50	600	14	1	511	0	1.37	1.42	2.08	0.66
G-847	50	600	7	1	511	0	1.37	0.68	0.40	-0.28
G-948	50	600	26	1	511	0	1.37	1.30	1.68	0.38
G-841	50	600	19	1	511	10.36	1.37	9.42	0.92	-8.46
G-845	50	600	12	1	511	10.36	1.37	10.86	1.54	-9.26
G-950	100	800	10	1	511	10.36	1.37	10.17	-0.15	-10.27
G-951	100	800	25	1	511	10.36	1.37	10.79	2.36	-8.37
G-1005	100	750	11	1	511	0	1.37	0.71	-0.07	-0.78
G-1006	100	750	11	1	511	10.36	1.37	10.20	6.63	-3.54

*Calculated by using the ratio of masses

†Cl concentration reported in ppm (average, n = 10)

Abbreviations: Prg = pargasite

Table B4. Fractionation factor best fit equations

Exponential associate: $\mathbf{y = y0 + A1*(1 - e^{(-x/t1)}) + A2*(1 - e^{(-x/t2)})}$	
y0	-516.0651
A1	258.26724
t1	0.74439
A2	258.26724
t2	0.74439
Second order exponential decay: $\mathbf{y = y0 + A1*e^{(-(x-x0)/t1)} + A2*e^{(-(x-x0)/t2)}}$	
y0	-0.20995
x0	3.16667
A1	0.47552
t1	0.88056
A2	0.47552
t2	0.88056

References

Barnes J. D. and Cisneros M. (2012) Mineralogical control on the chlorine isotope composition of altered oceanic crust. *Chemical Geology* **326–327**, 51–60.

Barnes J.D., Paulick H., Sharp Z. D., Bach W. and Beaudoin G. (2009) Stable isotope (δ18O, δD, δ37Cl) evidence for multiple fluid histories in mid-Atlantic abyssal peridotites (ODP Leg 209). *Lithos* **110**, 83–94.

Barnes J. D., Selverstone J. and Sharp Z. D. (2006) Chlorine isotope chemistry of serpentinites from Elba, Italy, as an indicator of fluid source and subsequent tectonic history. *Geochemistry, Geophysics, Geosystems* **7**, n/a–n/a.

Barnes J. D. and Sharp Z. D. (2006) A chlorine isotope study of DSDP/ODP serpentinized ultramafic rocks: Insights into the serpentinization process. *Chemical Geology* **228**, 246–265.

Barnes J. D., Sharp Z. D. and Fischer T. P. (2008) Chlorine isotope variations across the Izu-Bonin-Mariana arc. *Geology* **36**, 883–886.

Barnes J. D., Sharp Z. D., Fischer T. P., Hilton D. R. and Carr M. J. (2009) Chlorine isotope variations along the Central American volcanic front and back arc. *Geochemistry, Geophysics, Geosystems* **10**, n/a–n/a.

Barnes J. D. and Straub S. M. (2010) Chorine stable isotope variations in Izu Bonin tephra: Implications for serpentinite subduction. *Chemical Geology* **272**, 62–74.

Bigeleisen J. and Mayer M. G. (1947) Calculation of Equilibrium Constants for Isotopic Exchange Reactions. *The Journal of Chemical Physics* **15**, 261–267.

Bonifacie Magali, Busigny V., Mével C., Philippot P., Agrinier P., Jendrzejewski N., Scambelluri M. and Javoy M. (2008) Chlorine isotopic composition in seafloor serpentinites and high-pressure metaperidotites. Insights into oceanic serpentinization and subduction processes. *Geochimica et Cosmochimica Acta* **72**, 126–139.

Bonifacie M., Charlou J. L., Jendrzejewski N., Agrinier P. and Donval J. P. (2005) Chlorine isotopic compositions of high temperature hydrothermal vent fluids over ridge axes. *Chemical Geology* **221**, 279–288.

Bonifacie M., Jendrzejewski N., Agrinier P., Coleman M., Pineau F. and Javoy M. (2007) Pyrohydrolysis-IRMS determination of silicate chlorine stable isotope compositions. Application to oceanic crust and meteorite samples. *Chemical Geology* **242**, 187–201.

Bonifacie M., Jendrzejewski N., Agrinier P., Humler E., Coleman M. and Javoy M. (2008) The Chlorine Isotope Composition of Earth's Mantle. *Science* **319**, 1518–1520.

Bonifacie M., Monnin C., Jendrzejewski N., Agrinier P. and Javoy M. (2007) Chlorine stable isotopic composition of basement fluids of the eastern flank of the Juan de Fuca Ridge (ODP Leg 168). *Earth and Planetary Science Letters* **260**, 10–22.

Bottinga Y. and Javoy M. (1973) Comments on oxygen isotope geothermometry. *Earth and Planetary Science Letters* **20**, 250–265.

Brantley S. L., Liermann L. J., Guynn R. L., Anbar A., Icopini G. A. and Barling J. (2004) Fe isotopic fractionation during mineral dissolution with and without bacteria. *Geochimica et Cosmochimica Acta* **68**, 3189–3204.

Campbell D. J. (1985) Fractionation of stable chlorine isotopes during transport through semipermeable membranes. *M.S. thesis, Univerity of Arizona*.

Carothers W. W., Adami L. H. and Rosenbauer R. J. (1988) Experimental oxygen isotope fractionation between siderite-water and phosphoric acid liberated CO_2-siderite. *Geochimica et Cosmochimica Acta* **52**, 2445–2450.

Chacko T., Cole D. R. and Horita J. (2001) Equilibrium Oxygen, Hydrogen and Carbon Isotope Fractionation Factors Applicable to Geologic Systems. *Reviews in Mineralogy and Geochemistry* **43**, 1–81.

Clayton R. N. (1981) Isotopic Thermometry. In *Thermodynamics of Minerals and Melts* (eds. R. C. Newton, A. Navrotsky, and B. J. Wood). Advances in Physical Geochemistry. Springer New York. pp. 85–109. Available at: http://link.springer.com/chapter/10.1007/978-1-4612-5871-1_5 [Accessed June 30, 2013].

Clayton R. N., Goldsmith J. R., Karel K. J., Mayeda T. K. and Robert C. N. (1975) Limits on the effect of pressure on isotopic fractionation. *Geochimica et Cosmochimica Acta* **39**, 1197–1201.

Clayton R. N., O'Neil J. R. and Mayeda T. K. (1972) Oxygen isotope exchange between quartz and water. *Journal of Geophysical Research* **77**, 3057–3067.

Deer W. A., Howie R. A. and Zussman J. (1966) An introduction to the rock-forming minerals.

Eggenkamp H. G. M., Kreulen R. and Koster Van Groos A. F. (1995) Chlorine stable isotope fractionation in evaporites. *Geochimica et Cosmochimica Acta* **59**, 5169–5175.

Giblin L. E., Blackburn W. H. and Jenkins D. M. (1993) X-ray continuum discrimination technique for the energy-dispersive analysis of fine particles. *Anal. Chem.* **65**, 3576–3580.

Godon A., Jendrzejewski N., Castrec-Rouelle M., Dia A., Pineau F., Boulègue J. and Javoy M. (2004) Origin and evolution of fluids from mud volcanoes in the Barbados accretionary complex. *Geochimica et Cosmochimica Acta* **68**, 2153–2165.

Horita J., Cole D. R. and Wesolowski D. J. (1996) Stable Isotope Partitioning In Brine-Gas-Mineral Systems Relevant to Geothermal Resources. *Reservoir Technology*.

Horita J., Driesner T. and Cole D. R. (1999) Pressure Effect on Hydrogen Isotope Fractionation Between Brucite and Water at Elevated Temperatures. *Science* **286**, 1545–1547.

Ito E., Harris D. M. and Anderson Jr. A. T. (1983) Alteration of oceanic crust and geologic cycling of chlorine and water. *Geochimica et Cosmochimica Acta* **47**, 1613–1624.

Jenkins D. M. and Bozhilov K. N. (2003) Stability and thermodynamic properties of ferro-actinolite: A re-investigation. *Am J Sci* **303**, 723–752.

John T., Scambelluri M., Frische M., Barnes J. D. and Bach W. (2011) Dehydration of subducting serpentinite: Implications for halogen mobility in subduction zones and the deep halogen cycle. *Earth and Planetary Science Letters* **308**, 65–76.

Kiczka M., Wiederhold J. G., Frommer J., Kraemer S. M., Bourdon B. and Kretzschmar R. (2010) Iron isotope fractionation during proton- and ligand-promoted dissolution of primary phyllosilicates. *Geochimica et Cosmochimica Acta* **74**, 3112–3128.

Krutov G. A. (1936) Dashkesanite, a new chlorine amphibole of the hastingsite group. *Mineral. Abstr* **6**, 438.

Layne G. D., Kent A. J. R. and Bach W. (2009) δ^{37}Cl systematics of a backarc spreading system: The Lau Basin. *Geology* **37**, 427–430.

Leake B. E., Woolley A. R., Arps C. E. S., Birch W. D., Gilbert M. C., Grice J. D., Hawthorne F. C., Kato A., Kisch H. J., Krivovichev V. G., Linthout K., Laird J., Mandarino J. A., Maresch W. V., Nickel E. H., Rock N. M. S., Schumacher J. C., Smith D. C., Stephenson N. C. N., Ungaretti L., Whittaker E. J. W. and Youzhi G. (1997) Nomenclature of amphiboles; Report of the Subcommittee on Amphiboles

of the International Mineralogical Association, Commission on New Minerals and Mineral Names. *American Mineralogist* **82**, 1019–1037.

Liebscher A., Barnes J. D. and Sharp Z. D. (2006) Chlorine isotope vapor–liquid fractionation during experimental fluid-phase separation at 400 °C/23 MPa to 450 °C/42 MPa. *Chemical Geology* **234**, 340–345.

Liu J., Liu W., Ye K. and Mao Q. (2009) Chlorine-rich amphibole in Yangkou eclogite, Sulu ultrahigh-pressure metamorphic terrane, China. *Eur J Mineral* **21**, 1265–1285.

Macris C. A., Young E. D. and Manning C. E. (2013) Experimental determination of equilibrium magnesium isotope fractionation between spinel, forsterite, and magnesite from 600 to 800 °C. *Geochimica et Cosmochimica Acta* **118**, 18–32.

Magenheim A. J., Spivack A. J., Michael P. J. and Gieskes J. M. (1995) Chlorine stable isotope composition of the oceanic crust: Implications for Earth's distribution of chlorine. *Earth and Planetary Science Letters* **131**, 427–432.

Matthews A., Goldsmith J. R. and Clayton R. N. (1983a) On the mechanisms and kinetics of oxygen isotope exchange in quartz and feldspars at elevated temperatures and pressures. *Geological Society of America Bulletin* **94**, 396–412.

Matthews A., Goldsmith J. R. and Clayton R. N. (1983b) Oxygen isotope fractionation between zoisite and water. *Geochimica et Cosmochimica Acta* **47**, 645–654.

Mazdab F. K. (2003) The Diversity and Occurrence of Potassium-Dominant Amphiboles. *Can Mineral* **41**, 1329–1344.

Morrison J. (1991) Compositional constraints on the incorporation of Cl into amphiboles. *American Mineralogist*, 1920–1930.

Munoz J. L. (1984) F-OH and Cl-OH exchange in micas with applications to hydrothermal ore deposits. *Reviews in Mineralogy and Geochemistry* **13**, 469–493.

Munoz J. L. and Swenson A. (1981) Chloride-hydroxyl exchange in biotite and estimation of relative HCl/HF activities in hydrothermal fluids. *Economic Geology* **76**, 2212–2221.

Northrop D. A. and Clayton R. N. (1966) Oxygen-Isotope Fractionations in Systems Containing Dolomite. *The Journal of Geology* **74**, 174–196.

O'Neil J. R. (1986) Theoretical and experimental aspects of isotopic fractionation. In Stable Isotopes in High Temperature Geological Processes. *Mineralogical Society of America, Washington, DC Rev. Mineral.* **16**, 1 – 40.

O'Neil J. R. and Taylor H. P. (1969) Oxygen isotope equilibrium between muscovite and water. *Journal of Geophysical Research* **74**, 6012–6022.

Oberti R., Ungaretti L., Cannillo E. and Hawthorne F. C. (1993) The mechanism of Cl incorporation in amphibole. *American Mineralogist* **78**, 746–752.

Parrington J. R., Knox H. D., Brennan S. L., Baum E. M. and Feiner R. (1966) *Nuclides and isotopes: chart of the nuclides*., General Electric Co. and KAPL, Inc.

Pearce C. R., Saldi G. D., Schott J. and Oelkers E. H. (2012) Isotopic fractionation during congruent dissolution, precipitation and at equilibrium: Evidence from Mg isotopes. *Geochimica et Cosmochimica Acta* **92**, 170–183.

Philippot P., Agrinier P. and Scambelluri M. (1998) Chlorine cycling during subduction of altered oceanic crust. *Earth and Planetary Science Letters* **161**, 33–44.

Polyakov V. . and Kharlashina N. . (1994) Effect of pressure on equilibrium isotopic fractionation. *Geochimica et Cosmochimica Acta* **58**, 4739–4750.

Ransom B., Spivack A. J. and Kastner M. (1995) Stable Cl isotopes in subduction-zone pore waters: Implications for fluid-rock reactions and the cycling of chlorine. *Geology* **23**, 715–718.

Richet P., Bottinga Y. and Javoy M. (1977) A Review of Hydrogen, Carbon, Nitrogen, Oxygen, Sulphur, and Chlorine Stable Isotope Fractionation Among Gaseous Molecules. *Annual Review of Earth and Planetary Sciences* **5**, 65–110.

Richter F. M., Mendybaev R. A., Christensen J. N., Hutcheon I. D., Williams R. W., Sturchio N. C. and Beloso Jr. A. D. (2006) Kinetic isotopic fractionation during diffusion of ionic species in water. *Geochimica et Cosmochimica Acta* **70**, 277–289.

Rizzo A. L., Caracausi A., Liotta M., Paonita A., Barnes J. D., Corsaro R. A. and Martelli M. (2013) Chlorine isotope composition of volcanic gases and rocks at Mount Etna (Italy) and inferences on the local mantle source. *Earth and Planetary Science Letters* **371–372**, 134–142.

Saccocia P. J., Seewald J. S. and Shanks III W. C. (2009) Oxygen and hydrogen isotope fractionation in serpentine–water and talc–water systems from 250 to 450 °C, 50 MPa. *Geochimica et Cosmochimica Acta* **73**, 6789–6804.

Schauble E. A. (2004) Applying Stable Isotope Fractionation Theory to New Systems. *Reviews in Mineralogy and Geochemistry* **55**, 65–111.

Schauble E. A., Rossman G. R. and Taylor Jr. H. . (2003) Theoretical estimates of equilibrium chlorine-isotope fractionations. *Geochimica et Cosmochimica Acta* **67**, 3267–3281.

Selverstone J. and Sharp Z. D. (2011) Chlorine isotope evidence for multicomponent mantle metasomatism in the Ivrea Zone. *Earth and Planetary Science Letters* **310**, 429–440.

Sharp Z. D. (2007) *Principles of stable isotope geochemistry*., Pearson Education Upper Saddle River, NJ, USA.

Sharp Z. D., Barnes J. D., Brearley A. J., Chaussidon M., Fischer T. P. and Kamenetsky V. S. (2007) Chlorine isotope homogeneity of the mantle, crust and carbonaceous chondrites. *Nature* **446**, 1062–1065.

Sharp Z.D., Barnes J. D., Fischer T. P. and Halick M. (2010) An experimental determination of chlorine isotope fractionation in acid systems and applications to volcanic fumaroles. *Geochimica et Cosmochimica Acta* **74**, 264–273.

Sharp Z. D., Shearer C. K., McKeegan K. D., Barnes J. D. and Wang Y. Q. (2010) The Chlorine Isotope Composition of the Moon and Implications for an Anhydrous Mantle. *Science* **329**, 1050–1053.

Skulan J. L., Beard B. L. and Johnson C. M. (2002) Kinetic and equilibrium Fe isotope fractionation between aqueous Fe(III) and hematite. *Geochimica et Cosmochimica Acta* **66**, 2995–3015.

Spivack A. J., Kastner M. and Ransom B. (2002) Elemental and Isotopic Chloride Geochemistry and Fluid Flow in the Nankai Trough. *Geophysical Research Letters* **29**, 6–1–6–4.

Staudigel H. (2003) 3.15 - Hydrothermal Alteration Processes in the Oceanic Crust. In *Treatise on Geochemistry* (eds. Editors-in-Chief: Heinrich D. Holland and Karl K. Turekian). Pergamon, Oxford. pp. 511–535. Available at: http://www.sciencedirect.com/science/article/pii/B0080437516030322 [Accessed July 12, 2013].

Straub S. M. and Layne G. D. (2003) The systematics of chlorine, fluorine, and water in Izu arc front volcanic rocks: Implications for volatile recycling in subduction zones. *Geochimica et Cosmochimica Acta* **67**, 4179–4203.

Thomas W. M. (1982) Stability relations of the amphibole hastingsite. *Am J Sci* **282**, 136–164.

Turekian K. K. and Wedepohl K. H. (1961) Distribution of the Elements in Some Major Units of the Earth's Crust. *Geological Society of America Bulletin* **72**, 175–192.

Urey H. C. (1947) The thermodynamic properties of isotopic substances. *J. Chem. Soc.*, 562–581.

Vanko D. A. (1986) High-chlorine amphiboles from oceanic rocks; product of highly-saline hydrothermal fluids? *American Mineralogist* **71**, 51–59.

Volfinger M., Robert J.-L., Vielzeuf D. and Neiva A. M. R. (1985) Structural control of the chlorine content of OH-bearing silicates (micas and amphiboles). *Geochimica et Cosmochimica Acta* **49**, 37–48.

Weidner J. (1989) Welding silver and silver alloy containers for high-temperature and high-pressure experiments. *American Mineralogist* **74**, 1385.

Wiberg N. (2001) Holleman-Wiberg's inorganic chemistry. *Academic Press, New York*.

Wiederhold J. G., Kraemer S. M., Teutsch N., Borer P. M., Halliday A. N. and Kretzschmar R. (2006) Iron Isotope Fractionation during Proton-Promoted, Ligand-Controlled, and Reductive Dissolution of Goethite. *Environ. Sci. Technol.* **40**, 3787–3793.

Yapp C. J. (1990) Oxygen isotopes in iron (III) oxides: 1. Mineral-water fractionation factors. *Chemical Geology* **85**, 329–335.

Zheng Y.-F. (1993) Calculation of oxygen isotope fractionation in hydroxyl-bearing silicates. *Earth and Planetary Science Letters* **120**, 247–263.

Zhu C., Xu H., Ilton E. S., Veblen D. R., Henry D. J., Tivey M. K. and Thompson G. (1994) TEM-AEM observations of Cl-rich amphibole and biotite and possible petrologic implications. *American Mineralogist* **79**, 909–920.